Chapter 4 in Transport Phenomena in Fuel Cells, B. Sundén & M. Faghri (eds), pp. 133-174, WIT Press, ISBN 1-85312-840-6, 2005.

On heat and mass transfer phenomena in PEMFC and SOFC and modeling approaches

J. Yuan[1], M. Faghri[2] & B. Sundén[1]
[1]*Division of Heat Transfer,*
Lund Institute of Technology, Sweden.
[2]*Department of Mechanical Engineering and Applied Mechanics,*
University of Rhode Island, USA.

Abstract

There are similarities among various transport processes in solid oxide fuel cells (SOFCs) and proton exchange membrane fuel cells (PEMFCs), but also some differences. The present work concerns modeling and numerical analysis of heat, mass transfer/species flow, two-phase transport and effects on the cell performance in SOFCs and PEMFCs. Numerical calculation methods are further developed to enable predictions of convective heat transfer and pressure drop in flow ducts of the fuel and the oxidant. The unique boundary conditions (thermal, mass) for the flow ducts in fuel cells are identified and implemented. The composite duct consists of a porous layer, gas flow duct and/or solid current inter-connector (or -collector). The results from this study are applicable for other investigations considering overall fuel cell modeling and system studies, as well as the emerging field of micro-reactor engineering.

1 Introduction

In a fuel cell, electrical energy is generated directly through the electrochemical reaction of oxidant (oxygen from air) and fuels (such as natural gas, methanol, or pure hydrogen) at two electrodes separated by an electrolyte. When pure hydrogen is used, the only products of this process are heat, electricity and water. Unlike a battery, fuel cells do not store energy. The energy conversion is achieved without making use of the materials that constitute an integral part of the fuel cell structure. It should be noted that fuel cells convert chemical energy directly into electricity without an intermediate combustion process.

One of the main factors that have influenced the development of fuel cells has been the increasing concern about the environmental consequences of fossil fuel utilization in the production of electricity and for the propulsion of vehicles. More importantly is the increasing global awareness of how industry activities influence the environment and how a sustainable energy development can be achieved with a tremendously increasing world population. Fuel cells may help to reduce our dependence on fossil fuels and diminish poisonous emissions into the atmosphere.

The operation of a fuel cell requires a fuel electrode (*Anode*), oxidant electrode (*Cathode)*, electrically-insulating ionic conductor (*Electrolyte*), and external electric circuit. In general, fuel cells can be classified according to the type of ionic conductor (*Electrolyte*) they use and the temperature range at which they operate.

Several types of fuel cells are currently under development. Alkali fuel cells (AFCs) use alkaline potassium hydroxide as the electrolyte, and have been used for a long time by NASA on space missions. In proton exchange membrane fuel cells (PEMFCs) and phosphoric acid fuel cells (PAFCs), hydrogen fuel dissociates into free electrons and protons (positive hydrogen ions). The hydrogen protons migrate through the electrolyte to the cathode. The liquid-fed direct methanol fuel cell (DMFC) feeds a solution of methanol and water to the anode. At the cathode, oxygen from air, electrons from the external circuit and protons combine to form pure water and heat. All these three types are low temperature fuel cells. High temperature fuel cells, such as solid oxide fuel cells (SOFCs) and molten carbonate fuel cells (MCFCs) are of particular interest, because their high temperature operation allows natural gas to be used as a fuel, and the hybrid concept involving a combination of a fuel cell and a gas turbine becomes feasable. The overall system efficiency can be significantly increased in a hybrid system. Operation at a temperature of about 1000 ^{o}C (conventional, electrolyte-supported planar design), 700 ^{o}C (intermediate temperature, anode-supported design) and pressures greater than one atmosphere leads to solid oxide fuel cells (SOFCs) as one of the choices. It has been found that the proton exchange membrane fuel cell (PEMFC) system has some advantages, such as its relative simplicity of design and operation, low cost construction and self-starting at low temperatures. Both SOFC and PEMFC systems are expected to play a significant role in the next generation of primary or auxiliary power for stationary, portable, and automotive systems.

During the last decades, a large amount of research activities have been carried out on fuel cells worldwide, with particular interest and focus on SOFC and PEMFC systems. High performance, low cost and high reliability have been considered as the primary aspects and concerns for fuel cells to compete with well-developed fossil fuel power technology, such as the internal combustion engine. Most of the work has focused on creating new materials and material processes for the manufacturing of specific systems so as to achieve good cell/stack performance while minimizing the final system cost and size. To help expand future market opportunities for fuel cells, additional fundamental understanding and research work are needed. More attention needs to be focused on detailed analysis of transport processes, even at micro scale level. Because of

the particular sensitivities and complexities of fuel cells, analysis and optimization of fuel cell components/system can effectively be performed by numerical modeling and simulation.

The present work concerns numerical analysis of heat and mass transport processes, and fluid flow in ducts of both planar type solid oxide fuel cells and proton exchange membrane fuel cells. Numerical models have been developed to enable predictions of convective heat transfer and pressure drop in flow ducts of the fuel and the oxidant. The composite duct consists of a porous layer, gas flow duct and/or solid current inter-connector (or collector). The results from this study are applicable for related investigations considering overall fuel cell modeling and system studies, e.g., by providing heat transfer coefficients for various conditions, as well as in the emerging field of micro-reactor engineering. In general, the work also contributes to the understanding of duct flow.

2 Fuel cell modeling development

Despite the differences in terms cell structure/materials employed and operating conditions (such as temperature, pressure), supply of species to an active surface of cells in the stack is a common feature of fuel cells, such as SOFCs and PEMFCs. It is so because the performance degradation for the cells operating within the stack results from the unequal distribution of reactant mass flow among the cells. Understanding the various gas and heat transport processes is crucial for increasing the power density, reducing manufacturing costs and accelerating commercialisation of fuel cell systems. To this end, detailed modeling and improved simulation tools are required to fully characterize the complex multi-dimensional, multi-phase and multi-component transport processes on media that are both porous and electrochemically reactive.

2.1 Basics of SOFCs and PEMFCs

There are various similarities in the transport processes occurring in SOFCs and PEMFCs. In the anode duct, the fuel (e.g., H_2) is supplied and air ($O_2 + N_2$) is introduced in the cathode duct, and these ducts are separated by the electrolyte/electrode assembly. Reactants are transported by diffusion and/or convection to the electrode/electrolyte (SOFC) or catalyst/electrolyte (PEMFC) interfaces, where electrochemical reactions take place. An electrochemical oxidation reaction at the anode produces electrons that flow through the inter-collector (bipolar plate, for PEMFC) or -connector (for SOFC) to the external circuit, while the oxide ions (in SOFCs) or protons (in PEMFCs) pass through the electrolyte to the opposing electrode. The electrons return from the external circuit to participate in the electrochemical reaction at the cathode. In the electrochemical reaction process, part of the oxygen is consumed in the cathode duct, while the hydrogen is consumed in the anode duct. Heat and water (H_2O) are the only by-products during the process. The water generated is injected into

the anode duct further along the duct in SOFCs, while in PEMFCs, it enters into the cathode duct. The electrochemical reactions in SOFCs can be written as:

Cathode reaction: $$\tfrac{1}{2}O_2 + 2e^- \rightarrow O^{2-} \quad (1a)$$

Anode reaction: $$H_2 + O^{2-} \rightarrow H_2O + 2e^- \quad (1b)$$

and for PEMFCs:

Cathode reaction: $$\tfrac{1}{2}O_2 + 2e^- + 2H^+ \rightarrow H_2O \quad (2a)$$

Anode reaction: $$H_2 \rightarrow 2H^+ + 2e^- \quad (2b)$$

The overall reaction is as follows:

$$\tfrac{1}{2}O_2 + H_2 \rightarrow H_2O \quad (3)$$

Due to the flow resistance in the fuel cells, the pressure drop (ΔP) along the ducts and in the manifolds can cause non-uniform flow distribution. Furthermore, the output of electrical energy will differ in terms of voltage potential and in some cases even gas re-circulation occurs. At some severe conditions, the lack of gas in some channels can cause the irreversible damage to the fuel cell components. The pressure drop depends on the channel and manifold structures, flow streams etc. However, the temperature is always non-uniform even when there is a constant mass flow rate in the ducts. This is caused by the heat transfer and phase change (in PEMFCs), which in turn causes fluctuation in the available ΔT. Heat transfer occurs in the following manner:

- Between the cell component layers and the flowing air and fuel streams. This can be described in terms of heat transfer coefficients h_a (for air channel), h_f (for fuel channel) due to forced convective heat transfer with or without natural convection;
- Between the fuel and air streams across the interconnect layer in terms of the overall heat transfer coefficient, U;
- In solid structures in terms of heat conduction with different thermal conductivities, k_i (i = electrolyte, electrodes and current interconnect layers).

For the electrolyte and porous layers, often referred to as the membrane electrode assembly (MEA) in PEMFCs, the overall principal energy balance can be written as:

$$Q_c + h_f A_f (T_e - T_{f,av}) + h_a A_a (T_e - T_{a,av}) = Q_s \quad (4)$$

where Q_c is the heat conduction in the solid structure, Q_s is the heat source to account for the electrochemical heat generation, ohmic heating caused by the

electrical resistance due to the current flow; h is the convective heat transfer coefficient; T is the temperature. Equation (4) shows that the heat transfer coefficients in the fuel and oxidant ducts are important.

There are certainly some specific aspects and phenomena which need to be carefully investigated for different applications. As an example, Nafion® membranes are often employed in the electrolytes in PEMFCs. These membranes possess high ion conductivity by selecting perfluorosulphonic acid copolymers with a short pendant group. However, the performance of the membranes, in terms of electrical conductivity, strongly depends on the water content. Water management in the membrane is one of the major issues in PEMFCs. As discussed later in this chapter, there are several factors affecting the water content in the membrane, such as the water drag through the electrolyte (electro-osmotic), back diffusion of product water from the cathode to the anode. For the case of excessive accumulation of water vapor in the cathode, condensation may occur. Consequently, different methods of water management have been proposed and investigated. Another issue is the temperature range in which the membranes are stable. Therefore, both water and thermal management are coupled and need to be carefully balanced, as will be discussed later.

SOFCs employ solid oxide material as electrolyte and are, therefore, more stable. There are no problems with water management, liquid water flooding in the cathodes or slow oxygen reduction kinetics in SOFCs. On the other hand it is difficult to find suitable materials for operation at high temperatures.

There are other processes which only occur in SOFCs, such as internal reforming of fuels as pure hydrogen is not used and co-generation of heat/electricity with other power systems (such as gas turbines). For PEMFCs, external reforming is needed to handle hydrocarbon fuels. It should be mentioned that the reforming issues are not treated in this chapter but instead focus is on the composite duct flows in SOFCs and PEMFCs.

2.2 Modeling development

Modeling has already played an important role in fuel cell development since it facilitates a better understanding of parameters affecting the performance of fuel cells and fuel cell systems. Moreover, water management within the cathode is a key consideration in the design of the PEMFCs. However knowledge of the behavior of liquid water in electrodes is limited by the inability to make in situ measurements. Better understanding of the transport of water in the PEMFC electrode can be obtained from models that capture the important physical processes. This is particularly evident in works published in the open literature during recent years. There has been a range of models developed, from simple lumped models of individual cell channels to more complex three-dimensional detailed ones of complete stacks.

2.2.1 Modeling approaches

There are several issues which affect the choice of modeling strategies, and should be considered before selecting a fuel cell modeling approach. The most

important factors are the objectives and features of the model, which should be clearly defined and specified. These include the following issues, such as steady-state/transient, theoretical/semi-empirical, components/system study, lumped/ multidimensional, accuracy/time/flexibility, validation/documentations and so on. The development of modeling and simulation tools is a cost and time consuming process. The level of user knowledge and available resources (such as personnel and computer facilities etc.) are also constraints to include in the decision process.

Based on detailed electrochemical, fluid dynamics, species/current transport and heat transfer relationships, a theoretical fuel cell modeling approach usually employs the basic equations, such as the Stefan-Maxwell equation for gas-phase transport, and the Butler-Volmer equation for cell voltage [1]. The electrochemical and transport processes are tightly coupled. For proper water and thermal management, this approach includes not only the electrochemical reaction but also thermal- and fluid-dynamic equations. Multi-component species transport and heat transfer are important for providing a detailed picture of all processes in the fuel cell and the system. The output of the study can provide details of the processes, such as fuel cell species distribution/flow pattern, current density/temperature distribution, voltage and pressure drop, etc. On the other hand, based on experimental data specific to the applications and operating conditions, semi-empirical fuel cell models have also been developed during the recent years. Both approaches have advantages and disadvantages. The theoretical modeling approach is flexible to applications and operating conditions, and may be appreciated when detailed studies are desired. However, development and implementation of this approach takes a longer time, and it is difficult to validate due to lack of detailed data in the open literature. At present, the most readily available data are simply the overall *I-V* characteristics for a cell or stack. While the semi-empirical approach is already validated to some extent, it does not provide sufficient details. It should also be noted that it must be modified for each new application or operating conditions, and may not be suitable in some cases.

During recent years, reliable commercial fuel cell codes (or in some cases, a fuel cell module added to an already existing software) have been developed. For instance, detailed SOFC and PEMFC models have been included in the Chemical Engineering Module of FEMLAB, based on the platform of the MathWorks simulation code MATLAB [2]. More detailed modules associated with other commercial codes are being further developed and will be incorporated into standard cell and stack modeling when they have been validated.

2.2.2 Various existing models

In the last few years, attempts to simulate the velocities, pressures, temperatures, mass fractions, electric currents and potentials in fuel cells with given boundary conditions have been presented. This section only covers literature dealing with the relevant problems of heat transfer and gas flow modeling in SOFCs and PEMFCs.

2.2.2.1 SOFC modeling. For conventional electrolyte-supported planar structure, Vayenas [3] created a two-dimensional mixing cell model for cross-flow to simulate the distribution of gas species, temperature, and current density. For a unit cell with square and rectangular ducts, constant temperature was assumed for the solid walls, and the gas-phase composition was uniform. Another model was developed by Ahmed *et al.* [4]. This could be used to simulate the electrochemistry and thermal hydraulics in a cross-flow monolithic SOFC with alternating layers of anode, electrolyte, cathode, and interconnect. Based on the average thermal and compositional conditions, a Nusselt number (= hd/k) of 3.0 based on the equivalent diameter of the rectangular flow ducts was used for the convective heat transfer between the gases and the solid surfaces. In this model, the generated heat was released in the electrolyte, and the pressure drop in the channels was modeled by assuming fully developed laminar flow.

Bernier *et al.* [5] proposed a three-dimensional mathematical model to compute the local distribution of the electrical potential, temperature, and concentration of the chemical species. In the gas ducts, the thermal flux is mainly convective and conductive from the duct walls to the other solid parts. A computer code was developed by Melhus and Ratkje [6], which was used to find simultaneous solutions of all conservation equations for mass, energy and momentum in a quasi three dimensional simulation for single flat SOFCs. The reduction of the mass of O_2 in the cathode chamber was assumed to be regained in the anode as H_2O for the mass balance. Regarding the distribution of the gas flow, Boersma and Sammes [7] developed a model to simulate the non-uniform gas flow distribution along the height of a fuel cell system.

For the anode-supported design, the porous anode usually has a thickness of 1.5~2 mm [8~11], which is the thickest component and supporting structure, while a thin layer of electrolyte (~10 μm) is deposited on its surface. The transport path length for the fuel gases from the flow duct to the anode/electrolyte interface where the electrochemical reaction happens, is at least equal to the porous anode thickness. The transport rate of fuel gases is controlled by the porous layer microstructure (e.g., pore size, permeability, and porosity), pressure gradient between the flow duct and porous layer, gas composition, etc. There are various polarizations or losses (such as ohmic, activation and concentration) affecting the overall performance of SOFCs. It has been revealed that one of the principal losses in this design is attributed to concentration polarization caused by limitation of gaseous species transport through the porous anode [8], because the size of the porous anode might be bigger than that of the flow duct.

2.2.2.2 PEMFC modeling. It has been found that the proton exchange membrane fuel cell system has some advantages, such as its relative simplicity of design and operation, low cost construction materials and self-starting at low temperatures. However, water management is a critical issue for PEMFC, i.e., a high water-content must be maintained in the membrane in order to obtain acceptable ion conductivity. Water molecules are transferred from the anode duct to the cathode duct of the membrane by electro-osmosis during PEMFC operations. If this transport rate of water is higher than that of back diffusion, the

anode gases will dry out, and the membrane becomes dehydrated and too resistive to conduct current. On the other hand, cathode flooding occurs when the water removal rate fails to reach its minimum transport rate, which is caused by both the transport from the anode duct mentioned above and the generation of water by the electrochemical reaction H^+/O_2 at the catalyst surface [12]. Consequently, a sufficient amount of water must be supplied to the anode duct to make up for the loss due to net water transfer from the anode, and water should be removed at a sufficient rate from the cathode duct to keep an active catalyst surface for reaction.

Another challenging issue in PEMFCs is thermal management. In order to prevent excessive operating temperature and drying out of the membrane, the heat generated by the electrochemical reaction should be removed properly. The thermal management has a strong impact on the fuel cell performance, by affecting the transport of water and gaseous species as well as the electrochemical reactions in the cells. Both thermal and water management of PEMFCs are unique compared to other types of fuel cells.

Various water and/or thermal management systems have been claimed to be efficient by different approaches of humidification designs (injection of liquid/vapor water) and operating conditions [13~17] and anode water removal [18]. It should be noted that most of the models are one- or two-dimensional, and are limited by the isothermal assumptions and also neglect the potentially significant gas pressure drop within the electrodes. However, these studies provided a fundamental framework to build multi-dimensional and multi-component models, such as a fully three-dimensional [19~20], some of which include the heat transfer effects on the overall performance of fuel cells [20]. More recently, researchers have started to investigate two-phase water flow, by taking into account effects of heat generation/transfer and/or pressure drop [21~25].

2.2.2.3 Other processes relevant to fuel cell modeling. In fuel cells, the gaseous reactant flows at both the cathode and anode are subject to fluid injection and suction along the porous interface to the electrolyte. However, such processes are often simulated as flow in porous wall ducts at constant heat flux boundary condition [26]. Because both heat transfer and pressure distributions are significantly affected, fluid flow and heat transfer in ducts with mass transfer in porous walls have received a great deal of attention in the past decades [26~28]. Hwang *et al.* [26] simulated flow and heat transfer in a square duct in the range of $-20.0 < Re_m < 20.0$, with boundary conditions of one porous wall subjected to a constant heat flux, while the other three walls were assumed to be adiabatic and impermeable.

A better understanding of thermal engineering applications is required when porous materials are present in the duct flow. Because of its simplicity and reasonable accuracy within a certain range of applications, the Darcy model has been used for the majority of the existing studies on gas flow and heat transfer in porous media. It has been found that the Darcy model has some limitations, and

inertial forces should be taken into account when the interstitial flow velocity (i.e., the flow through pores of a porous medium) is not small [29]. It was reported in [30] that heat transfer can be significantly affected by Darcy number and the thermal conductivity ratio (between thermal conductivity of the porous media and that of the fluid). Various types of interfacial conditions between a porous medium and a gas flow duct were analyzed in details for both gas flow and heat transfer in [31]. It was found that as some of the gas flow penetrates sideways into the porous layer, the remaining gas flows downstream at decreasing flow rates. The static pressure in such a duct changes along the main flow stream due to the following reasons: the friction between the gas flow and the internal surfaces of the duct creates pressure losses, and the mass permeation across the interface between the flow duct and the porous layer implies that mass and momentum are transferred to/from the porous layer [32]. The permeation process in the porous media is usually considered as an overall mass transport with a constant permeability.

2.2.2.4 Further challenges. As discussed above, various models have been developed and improved for both SOFCs and PEMFCs. However, the modeling improvements are still limited due to, among other things, the limited material data available in the open literature. At a minimum, temperature and/or concentration dependent electrical resistivity and electrochemical activation energies, as well as the diffusion characteristics of the porous materials are pre-requisites to model development. Another critical factor limiting modeling development is the lack of test data that can be used to validate models.

3. Main processes in SOFCs and PEMFCs

The major processes significant to fuel cell characteristics are similar in SOFCs and PEMFCs. These processes are the species transport, electrochemical reactions, electronic and ionic transport, and heat transfer and distribution. Figure 1 shows a unit cell structure of fuel cells (representing PEMFCs in this case). It includes various components, such as fuel and oxidant gas ducts, electrolyte (polymer electrolyte membrane for PEMFCs), anode and cathode diffusion layers, catalyst layers in between them, and current inter-conductors.

3.1 Gas transport

In a fuel cell stack, the gas transport processes consist of:

- The fuel and oxidant gases flow separately through the gas manifolds where no electrochemical reactions occur;
- The fuel and oxidant gases flow along cell ducts where there is absorption of the reactants and the injection of reactive products from/to active surface;
- In the porous layers (electrodes), transport of the reactant gases occur towards the catalyst layer (in PEMFCs), or active surfaces (in SOFCs), and the exhaust gases are rejected to the cell ducts through the open pores;
- The exhaust gases from each cell are discharged through the gas output manifolds.

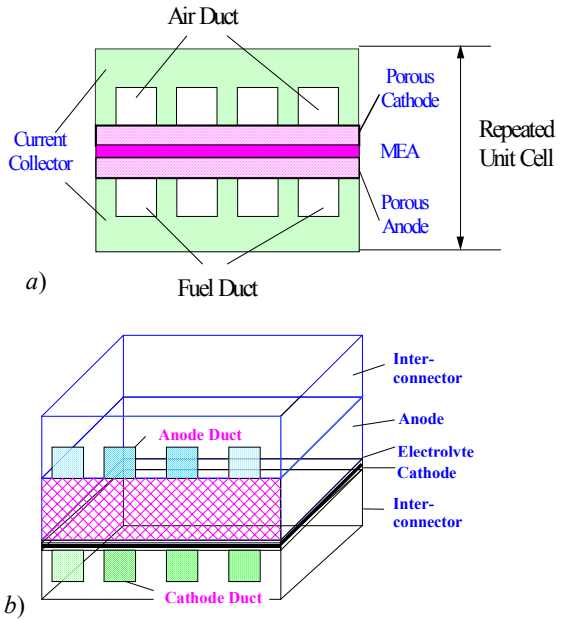

Figure 1: Schematic sketch of a unit cell for: *a*) PEMFC; and *b*) SOFC.

Fuel cell ducts and manifolds should be designed/configured to have appropriate gas flow rate and flow uniformity to the reactive surface. An important concern is the net pressure loss, which should be as low as possible to reduce parasitic power needed to operate pumps or compressors. Consequently, a laminar flow regime is effected in most of the fuel cells by employing small velocity and cross-sections in the manifolds and ducts [33].

The appropriate mass flow rate of reactants (fuels and oxidants) is determined by various factors, such as the requirement for the electrochemical reaction, proper thermal and water management, and fuel reforming reaction (SOFCs) etc. In PEMFCs, water management is critical to avoid the membrane dry out and cathode flooding. To deal with this concern, the oxidant flow rate may be increased to reduce the excess water generation.

3.2 Electrochemical reactions

At the active surface, the electrochemical reactions take place as described in eqns (1) and (2) for SOFCs and PEMFCs, respectively. The overall cell reaction is shown as eqn (3). The impacts of the electrochemical reactions on the gas mass balance are represented by the absorption of reactants and generation of products at the active surfaces, in terms of mass flux rate J (kg/m^{2}s). The mass flux rate is related to local current density I (A/m^2) and reads as follows when pure hydrogen is used as fuel.

- SOFC anode

$$J_{H_2} = -\frac{I}{2F} M_{H_2} \tag{5}$$

$$J_{H_2O} = \frac{I}{2F} M_{H_2O} \tag{6}$$

- PEMFC anode

$$J_{H_2} = -\frac{I}{2F} M_{H_2} \tag{7}$$

$$J_{H_2O} = -\frac{\alpha}{F} I \bullet M_{H_2O} \tag{8}$$

- SOFC cathode

$$J_{O_2} = -\frac{I}{4F} M_{O_2} \tag{9}$$

- PEMFC cathode

$$J_{O_2} = -\frac{I}{4F} M_{O_2} \tag{10}$$

$$J_{H_2O} = \frac{1+2\alpha}{2F} I \bullet M_{H_2O} \tag{11}$$

In the equations above, α is the net water transport coefficient, for the case of PEMFCs, which represents the net water transport through the membrane by electro-osmotic drag and back diffusion due to the water concentration difference, and hydraulic permeation due to the pressure difference between the two sides. Other symbols can be found in the nomenclature. It should be noted that negative sign (–) in the above equations represents gas consumption, while plus (+) means gas generation.

3.3 Heat transfer

As mentioned before, the heat transfer processes include various aspects, such as the convective heat transfer between the solid surface and the gas streams, conductive heat transfer in the solid and/or porous structures. Furthermore, heat generation occurs at the active surface in association with the electrochemical reactions and cell losses. The heat generation at the active surface, q_b, can be expressed as follows [20]:

$$q_b = -\frac{I}{2F} \Delta H_{H_2O} M_{H_2O} - I \bullet V_{cell} \tag{12}$$

where ΔH is the enthalpy change of formation of water. The first term on the RHS in the above equation accounts for the amount of heat energy released by the water formation, while the second one accounts for the current density

generated by the electrochemical reaction. When the inhomogeneous current density is taken into consideration, the total local heat generation must be defined due to local joule heating.

3.4 Various transport processes in the electrodes (porous layers)

Electrodes for fuel cells are generally porous to ensure maxium active surfaces, and to allow the injection of the generated products to the ducts. The mass transfer is dominated by the gas diffusion and/or convection, as discussed later in this chapter. This is ensured by the open pores of the electrodes, in terms of permeability and/or porosity. Another requirement of a porous electrode is to also have a good ionic conductivity, because the ionic particles are transported via the solid matrix of the porous layer. In general, the electrodes should have a balanced performance and long-time stability. In PEMFCs, a catalyst material is frequently employed, such as platinum or platinum/ruthenium, whereas SOFCs utilize much cheaper catalyst materials such as nickel due to reduced activation polarization at higher temperature.

3.5 Other processes appearing in fuel cell components

The electrolyte of fuel cells transport ions created by the electrochemical reaction at one electrode to the other. In PEMFCs the proton is transported through the electrolyte, while in SOFCs the oxygen ion is transferred. Reducing the electrolyte thickness and internal ohmic losses is a major requirement. On the other hand, the electrolyte should be impermeable to gases (fuel and oxidant) for the purpose of minimizing reactant crossover.

The cell inter-connectors or -collectors involve heat transfer by thermal conduction and current collection. Consequently, high electrical conductivity and thermal conductivity are the basic requirements. The materials having the following features are often employed, i.e., impermeability to reactants and chemically stable in oxidizing and reducing environments. In general, PEMFCs need more expensive materials, individually machined graphite or even gold-plated stainless steel materials.

It is well-known that the polarization curve, which represents the cell voltage behaviour against operating current density (*V-I* curve), is the standard measure of the performance for fuel cells, and depends on both the operating conditions and the component design. The operating conditions include the working temperature, partial pressures of fuel and oxidant and their utilization rate, and/or the water concentration in the components. On the other hand, the design parameters could be the porosity, tortuosity, thickness of the electrodes (concentration loss), thickness of the electrolyte (ohmic loss), and the electrode/electrolyte interface (activation loss).

4 Processes and issues in SOFC and PEMFC

Despite various similar processes discussed above, there are certainly processes and/or phenomena which are connected to a specific fuel cell type and should be

carefully considered. Among these, water management is a challenging issue for PEMFC, while internal fuel reforming at the anode side and high operating temperature have unique features relating to mass transport and heat transfer if fuels other than pure hydrogen are used in SOFCs. Moreover, thermal radiation may be important in SOFCs while it is not in PEMFCs.

4.1 Water management in PEMFCs

Polymer electrolyte membranes in PEMFCs are basically water filled to have high proton conductivity, as mentioned earlier. Factors influencing the water content in the electrolyte are generally two transport processes, i.e., water drag through the electrolyte membrane (a shell of H_2O is transported via the electrolyte for every proton transported), and back diffusion of generated water from the cathode into the anode through the electrolyte. The first one is often referred to as electro-osmotic transport in the literature, and the latter one is due to the gradient of water content in the electrolyte. The effective electro-osmotic coefficient α is an important parameter to represent water transport between the anode and the cathode. It includes the effects of both electro-osmosis and water back diffusion.

Water management in the electrolyte is one of the major issues in PEMFCs. This is because during PEMFC operation anode gases can be dried out if the electro-osmosis transport rate is higher than that of back diffusion, which consequently causes the electrolyte membrane to become dehydrated and too resistive to conduct current. On the other hand, water is generated at the cathode active surface and transported to the cathode duct. Cathode flooding may occur when the water removal rate fails to reach its threshold transport/generation rate. Both dry-out and water flooding should be avoided, and various water management schemes have been proposed. More detailed discussions on these issues can be found in [13~18]. It should also be noted that condensation can occur in the cathode duct when local vapor saturation condition occurs in the duct. As discussed later in this work, this case mainly happens at high current densities and low operating temperatures of fuel cells.

When such condensation occurs the transport process becomes two-phase, which besides flooding the cathode layer can considerably complicate the modeling procedure as no experimental results are available for two-phase flow in PEMFCs. Instead, much attention has been paid on numerical investigations to reveal the relationships between the water saturation, proton conductivity (ohmic loss), the level of catalyst flooding (activation loss), and the effective diffusivity of the porous layer (concentration loss); see [21~26].

4.2 Fuel reforming issues in SOFC

Because of the high operating temperature, an SOFC can convert not only hydrogen into electricity, but can also reform hydrocarbon compounds into reactant fuels. For instance, methane can be converted to H_2 and CO_2 in a steam reforming process within the anode of SOFCs. This reforming process takes

place at the surface and in a very thin layer of the anode porous nickel cermets (ceramic metal) [10]. It is often referred to as internal reforming in the literature.

The methane reforming reaction in this case can be written as follows:

$$CH_4 + H_2O \rightarrow CO + 3H_2 \qquad \Delta H = 206 \text{ kJ/mol} \qquad (13a)$$

$$CO + H_2O \rightarrow CO_2 + H_2 \qquad \Delta H = -41 \text{ kJ/mol} \qquad (13b)$$

Equation (13*b*) is usually referred to as water gas shift reaction. The overall reforming reaction is:

$$CH_4 + 2H_2O \rightarrow CO_2 + 4H_2 \qquad (13)$$

It should be mentioned that the above processes in eqn (13) are net endothermic and the overall balance of the reaction requires external heat input. This heat can be supplied by the exothermic electrochemical reaction, as given in eqns (1) and (2). Due to the fast reforming reaction compared to the electrochemical reaction, the endothermic steam reforming process may lead to local sub-cooling, and/or mechanical failure due to thermally induced stresses [10].

5 Modeling methodologies for transport processes in SOFC and PEMFC

5.1 General considerations

A typical configuration of a simulated fuel cell duct is shown in Figure 2. This section focuses on the establishment of equations for the analysis of the fuel cell ducts appearing in SOFCs and PEMFCs. The duct under study includes the gas flow duct, porous layer (anode/cathode) and solid current inter-connector or collector.

The variables to be solved for are the gas transport velocities in the x, y and z directions, the gas mass concentration/distribution, pressure drop, temperature distribution and convective heat transfer coefficient (in term of Nusselt number, Nu). The liquid water saturation and its effects on the current density distribution are modeled for PEMFCs.

The governing equations consisting of species (H_2, H_2O, O_2, etc.), momentum and energy equations, are solved for various sub-domains. Auxiliary equations are employed to calculate the source terms in the governing equations. A unified framework is developed for both SOFC and PEMFC, by implementing specific source terms to account for different transport processes and boundary conditions.

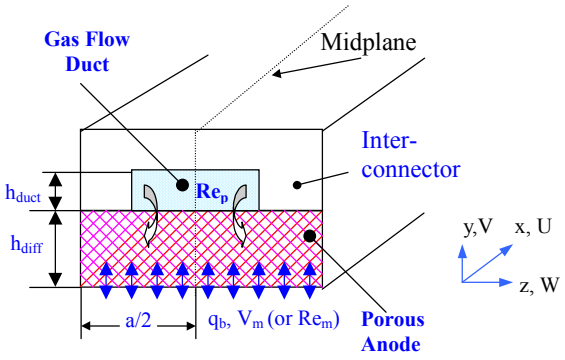

Figure 2: Schematic drawing of a composite fuel cell duct (Anode-supported planar SOFC) under consideration.

5.2 Assumptions

Steady laminar flow of incompressible fluid is considered. The appropriate mass flow rate of reactants is determined by several factors related to various requirements, e.g., maintaining proper water balance and thermal management. Water management concerns in PEMFCs may need an increased flow rate, which can be described by a parameter named the stoichiometric ratio for an electrode reaction. In general, the gas flow duct should be designed to minimize pressure drop, while providing adequate and evenly distributed mass transfer through the porous layer for the electrochemical reaction. Thus, typically laminar flow with *Re* numbers of the order of 100~1000 have been employed for fuel cells [33]. For simplicity, the following additional assumptions are applied:

- The inlet-velocity and axial-temperature distributions of the species are assumed uniform, and the inlet Reynolds number is assumed to be Re_{in} ($=U_{in}D_h/\nu$) >> 1;
- An electrochemical reaction is assumed to occur at the interface between electrodes and electrolyte. The released heat is simulated as a wall heat flux q_b at one duct wall (the bottom wall in Figure 2);
- When the porous layer is thick and needs to be considered (as for the ducts in PEMFCs and anode-supported SOFCs), it is assumed to be homogeneous and characterized by effective parameters, such as porosity, permeability and thermal conductivity, and the fluid in the porous layer is in thermal equilibrium with the solid matrix;
- Mass consumption and generation are simulated by a mass transfer flux (see following sections for more details);
- In PEMFCs, liquid water appears in the form of small droplets in the gas species. A multi-phase mixture model is employed to describe two-phase flow and heat transfer in the composite duct. This model enables the calculation of the individual phase velocities from the mixture flow field

when the capillary flow due to the pressure gradient and gravity-induced phase migration are considered. For simplicity, the interfacial shear force and surface tension force between the liquid water and the gas phase are neglected; liquid water has the same pressure as the gas species.

5.3 Governing equations

The governing equations to be solved are the continuity, momentum, energy and species equations. The mass continuity equation is written as

$$\nabla \bullet (\rho_{eff} \mathbf{V}) = S_m \tag{14}$$

The source term S_m in the above equation accounts for the mass balance caused by the reaction from/to the active surface A_{active} (bottom surface in Figure 2). For PEMFCs, it corresponds to the hydrogen and water consumption on anode side, oxygen consumption and water generation on the cathode side, respectively. These are given by [19, 20],

$$S_m = S_{H_2} + S_{a,H_2O} = (-\frac{I}{2F} M_{H_2} - \frac{\alpha}{2F} I \bullet M_{H_2O}) \frac{A_{active}}{V} \tag{15}$$

$$S_m = S_{O_2} + S_{c,H_2O} = (-\frac{I}{4F} M_{O_2} + \frac{(1+2\alpha)I}{2F} M_{H_2O}) \frac{A_{active}}{V} \tag{16}$$

where, V refers to control volume at the active site.

The momentum equation reads

$$\nabla \bullet (\rho_{eff} \mathbf{VV}) = -\nabla P + \nabla \bullet (\mu_{eff} \nabla \mathbf{V}) + S_{di} \tag{17}$$

The inclusion of the source term S_{di} allows eqn. (17) to be valid for both the porous layer and the flow duct

$$S_{di} = -(\mu_{eff} \mathbf{V} / \beta) - \rho_{eff} B V_i |\mathbf{V}| \tag{18}$$

The first term on the right hand side of the above equation accounts for the linear relationship between the pressure gradient and flow rate according to Darcy's law. The second term is the Forchheimer term which takes into account the inertial force effects, i.e., the non-linear relationship between pressure drop and flow rate. In eqn. (18), β is the porous layer permeability, and $\boldsymbol{V}$ represents the volume-averaged velocity vector of the species mixture. For example, the volume-averaged velocity component U in the x direction is equal to εU_p, where ε is the porosity, U_p the average pore velocity (or interstitial velocity). This source term accounts for the linear relationship between the pressure gradient and flow rate by the Darcy law. It should be noted that eqn (17) is formulated to

be generally valid for both the flow duct and the porous layer. The source term is zero in the flow duct, because the permeability β is infinite. Equation (17) then reduces to the regular Navier-Stokes equation. For the porous layer, the source term, eqn (18), is not zero, and the momentum eqn (17) with the non-zero source term in eqn (18) can be regarded as a generalized Darcy model.

The energy equation can be expressed as

$$\nabla \bullet (\rho_{eff} \mathbf{v} T) = \nabla \bullet \left(\frac{k_{eff}}{c_{peff}} \nabla T \right) + S_{wp} \tag{19}$$

where S_{wp} is the heat source associated with the water phase change (condensation/vaporization) for the case of PEMFC, see [20].

$$S_{wp} = J_{wl} \times h_{wl} \tag{20}$$

where J_{wl} is the mass flux of liquid water by phase change, and h_{wl} is the water latent heat.

The species conservation equations are formulated in the general equation,

$$\nabla \bullet (\rho_{eff} \mathbf{v} \phi) = \nabla \bullet (\rho_{eff} D_{\phi,eff} \nabla \phi) + S_{\phi} \tag{21}$$

where ϕ is the mass fraction. The above equation is solved for the mass fraction of H_2 in the case of an SOFC anode, and O_2, $H_2O^{(v)}$ and $H_2O^{(l)}$ in the case of a PEMFC cathode, respectively. The concentration of the inert species, nitrogen, is determined from a summation of the mass fractions of the other species. For PEMFC, the source term in eqn (21) includes water vapor and liquid water caused by the phase change. It is written as follows [20]

$$S_{wv} = -S_{wl} = M_{H_2O} \left(\frac{P_{w,sat} - P_{wv}}{P - P_{w,sat}} \right) \sum_i \left(\frac{mass_i}{M_i} \right) \tag{22}$$

In eqn. (22), $mass_i$ refers to mass of species i; P_{wv} refers to partial pressure of water vapor, $P_{w,sat}$ is the saturation pressure at the local temperature, while P is local pressure. If the partial pressure of water vapor is greater than the saturation pressure, water vapor will condense, and a corresponding amount of liquid water is formed. The water vapor partial pressure P_{wv} in the above equation is calculated based on its concentration and local pressure of the gas mixture, while the saturated pressure $P_{w,sat}$ at the local temperature reads [21],

$$\log_{10} P_{w,sat} = -2.179 + 0.029T - 9.183 \times 10^{-5} T^2 + 1.445 \times 10^{-7} T^3 \tag{23}$$

5.4 Boundary and interfacial conditions

A constant flow rate $U = U_{in}$ is specified at the inlet of the gas flow duct, while $U = 0$ is specified at the inlet and the outlet of the inter-connector (or collector) and porous layer. The other boundary conditions employed can be written as:

$$U = V - V_m = W = 0, -k_{eff}\frac{\partial T}{\partial y} = q_b,$$
$$-\rho_{eff} D_{\phi,eff}\frac{\partial \phi}{\partial y} = J_\phi \quad \text{at bottom wall } (y = 0) \tag{24}$$

$$U = V = W = 0,\ q = 0 \text{ (or } T = T_w),\ J_\phi = 0$$
$$\text{at top and side walls} \tag{25}$$

$$\frac{\partial U}{\partial z} = \frac{\partial V}{\partial z} = W = \frac{\partial T}{\partial z} = \frac{\partial \phi}{\partial z} = 0$$
$$\text{at mid-plane } (z = a/2) \tag{26}$$

It should be noted that all the walls for the above boundary conditions are on the external surfaces of the solid layer and porous layer. In eqn (24), V_m is the wall velocity of mass transfer caused by the electrochemical reaction, see eqns (1) and (2). The detailed procedure to obtain V_m was presented in [35], and the final form of the source term in eqn. (14) is given by

$$S_m = \rho_{eff}\ \mathrm{Re}_m \frac{\nu}{D_h}\frac{a}{A} \tag{27}$$

where $Re_m = V_m D_h/\nu$ is the wall Reynolds number caused by the electrochemical reaction. The other variables can be found in the nomenclature list. q_b in eqn (24) is the heat source caused by the reaction and was given in eqn (12), see [20].

Among various interfacial conditions between the porous layer and gas flow region, the continuity of velocity, shear stress, temperature, heat flux, mass fraction and flux of species (for the oxygen, water vapor and liquid water, respectively) are adopted, i.e.,

$$U_- = U_+,\ (\mu_{eff}\partial U/\partial y)_- = (\mu_f \partial U/\partial y)_+ \tag{28}$$

$$T_- = T_+,\ (k_{eff}\partial T/\partial y)_- = (k_f \partial T/\partial y)_+ \tag{29}$$

$$\phi_- = \phi_+,\ (\rho_{eff} D_{\phi,eff}\partial \phi/\partial y)_- = (\rho_{eff} D_{\phi,eff}\partial \phi/\partial y)_+ \tag{30}$$

Here the subscript + (plus) is for the fluid side, while – (minus) is for the porous layer side. Moreover, the thermal interfacial condition eqn (29) is also

applied at the interface between the porous layer and solid layer with k_s instead of k_{eff}.

5.5 Additional equations

It should be noted that the properties in the above equations with subscript *eff* are effective ones. For the flow duct, the effective properties are reduced to regular values of the species mixture based on the species composition, or regarded as constant values in some cases. In the porous layer, there are many factors affecting the effective properties such as the microstructure or nanostructure of the porous layer, species composition and local temperature etc. It is not easy to obtain more accurate values at this moment because the available data of the porous layer structure are still limited. It has been found that setting $\mu_{eff} = \mu_f$ and $\rho_{eff} = \rho_f$ provide good agreement with experimental data [43]. For the sake of simplicity, this approach is adopted here as well.

To reveal the porous layer effects, parameter studies can be carried out for the conductivity k_{eff} and species diffusion coefficients $D_{\phi,eff}$ by employing the ratios, θ,

$$\theta_k = k_{eff} / k_f \tag{31}$$

$$\theta_D = D_{\phi,eff} / D_\phi \tag{32}$$

In eqn (31), k_f is the species mixture conductivity in the porous layer, and is estimated by [39],

$$k_f = \frac{1}{2} \bullet \left[\sum_i x_i k_{fi} + \left(\sum \frac{x_i}{k_{fi}} \right)^{-1} \right] \tag{33}$$

where x_i is the mole fraction, and k_{fi} conductivity of the species component. The diffusion coefficients D_ϕ in eqn (32) are the values of the species components in the species mixture, i.e., D_{O_2}, $D_{H_2O}^{(v)}$ and $D_{H_2O}^{(l)}$ for oxygen, water vapor and liquid water, respectively. However, the binary diffusion coefficients of the components in pure air are used as estimations of D_ϕ in the calculations [23].

For the case of PEMFC, the effective diffusivity ratios are corrected by applying the so-called Bruggemann correction [23, 24] to account for the effects of porosity in the porous layer,

$$\theta_D = \varepsilon^{1.5} \tag{34}$$

It should be noted that the thermal physical properties of the species mixture, such as the density ρ_f, viscosity ν_f are estimated as functions of the local concentration.

According to Dalton's law, the relative humidity of the species mixture is defined as

$$\eta = \frac{P_{wv}}{P_{w,sat}} = x_{wv}\,\frac{P}{P_{w,sat}} \tag{35}$$

where P is the pressure, P_{wv} the water vapor partial pressure, $P_{w,sat}$ the saturation pressure identified in eqn (23), x_{wv} water vapor molar fraction. The liquid phase saturation s is employed to describe the liquid water volume fraction in the species mixture. It reads [21]

$$s = \frac{\rho\phi_w - \rho_g\phi_{wv}}{\rho_{wl} - \rho_g\phi_{wv}} \tag{36}$$

where ϕ is mass fraction, ρ_g gas phase density, ρ_{wl} liquid phase density. The density of the two-phase species mixture is

$$\rho = \rho_g(1\text{-}s) + \rho_{wl}s \tag{37}$$

5.6 Solution methodology

Due to the similarity of the conservation equations for SOFC and PEMFC, eqns (14, 17, 19, 21) can be written in the general form as

$$\nabla \bullet \left(\rho_{eff}\,\mathbf{V}\Phi\right) = \nabla \bullet \left(\Gamma_{\Phi,eff}\,\nabla\Phi\right) + S_\Phi \tag{38}$$

where Φ denotes any of the dependent variables, Γ is the diffusivity and S is a source term or sink term.

Because there is no analytical solution to eqn (38), computational fluid dynamics (CFD) methods have to be employed to obtain the discrete solutions. Once in this form, the equations are integrated over control volumes. The boundary conditions are introduced as source terms in control volumes neighboring boundaries whenever appropriate. Details of various numerical schemes can be found in [34].

The numerical analysis, performed in this chapter, has been conducted by developing various source terms/boundary conditions related to the fuel cell transport processes, and implementation into general purpose and in-house developed CFD codes. The finite-volume method is used in the codes. More detailed discussion on the codes can be found in [35].

It should be noted that the source term in eqn (14) (accounting for mass transfer effects) is zero in most of the regions, and non-zero only in the regions neighboring boundaries, where mass transfer caused by the electrochemical reaction occurs (bottom wall in Figure 2). The CFD procedures are modified accordingly and the source term S_m is implemented in the pressure correction

equation to adjust the mass balance due to mass transfer. For the composite duct, it is clear that no gas flow is present in the solid inter-connector (or -collector). Equations (17) and (21) are solved by applying high viscosity values and only the heat conduction equation, derived from the energy eqn (19), is solved for this domain.

In order to evaluate the performance of the numerical method and codes, test calculations considering grid sensitivity, code performance and validation have been carried out. These results can be found in [35] and the literature cited there. Due to the lack of experimental data for fuel cells, it should be mentioned that the computational codes have been validated by comparisons with fully developed/developing conditions in pure duct flow with mass transfer and ducts for various thicknesses of the porous layer.

6. Results and discussions

In the first section, dimensionless pressure differences and convective heat transfer coefficients, represented by friction factors and Nusselt numbers, respectively, are presented for conventional SOFC design, i.e., the porous electrodes (anode/cathode) are very thin and negligible, compared to the flow ducts. For the PEMFC and anode-supported SOFC design, the porous layer is thick and should be included in the analysis. The importance of gas flow and heat transfer in the porous layer and the effects on the transport processes in the flow duct are presented and discussed. For simplicity, the thermal boundary condition *TBC-I* refers to that of the constant heat flux at one wall, and constant temperature at the other three walls. *TBC-II* refers to the combination of constant heat flux at one wall, and thermal insulation at the remaining walls.

6.1 Mass transfer effects on the gas flow and heat transfer

For electrolyte-supported SOFC ducts, an overall mass balance is considered for the flow duct when the species consumption and generation happen in a fully developed flow.

$$\dot{m}_{in} + \dot{m}_m = \dot{m}_{out} \tag{39}$$

where $\dot{m}_m$ is the mass flow rate from the active wall caused by the electrochemi-cal reaction. Because Re_m ($=V_m D_h/\nu$) is assumed to be very small compared to the main flow Reynolds number, the mass transfer rate $\dot{m}_m$ is given by:

$$d\dot{m}_m = \rho a V_m dx \tag{40}$$

in which, dx is the increment in the main flow direction. The change of mass flow rate due to the mass transfer (suction/injection) reads:

$$d\dot{m} = \rho A\left(U_{bulk} + \frac{\partial U_{bulk}}{\partial x}dx\right) - \rho A U_{bulk} = \rho A \frac{\partial U_{bulk}}{\partial x}dx \tag{41}$$

By combining eqns. (40) and (41), the mass flow rate change can be written [35].

$$S_m = \rho \frac{\partial U_{bulk}}{\partial x} = \rho \mathrm{Re}_m \frac{v}{D_h}\frac{a}{A} \tag{42}$$

where $\partial U_{bulk}/\partial x$ is the velocity gradient in the main flow direction induced by the mass transfer. To characterize the overall pressure difference between inlet and outlet, either a pressure coefficient C_p or an apparent friction factor f_{app} of the gas flow in a duct can be employed as

$$C_p = \frac{(P_{in} - P)}{(\rho U_{bulk}^2 / 2)} \tag{43a}$$

$$4 f_{app} = \frac{D_h}{(\rho U_{bulk}^2 / 2)}\frac{dP}{dx} \tag{43b}$$

where U_{bulk} is the mean velocity of the main flow, D_h is the hydraulic diameter defined in the conventional manner, dP/dx the pressure gradient along the main flow direction.

The bulk velocity is calculated as:

$$U_{bulk} = \frac{\int U dA}{\int dA} \tag{44}$$

and the hydraulic diameter is defined as:

$$D_h = \frac{4A}{P^*} \tag{45}$$

A is the cross-sectional area and P^* is the wetted perimeter. It is clear that the mass transfer contributes to a change of the main flow velocity, thus the local Reynolds number varies as a function of x and mass flow rate even when the flow is fully-developed. It should be noted that the fluid pressure is affected by inertia forces and wall friction. As an example, the pressure difference increases for the case of injection, and it is larger than for the case without mass transfer. The apparent friction factor f_{app} is employed in this study because it incorporates the combined effect of wall shear and the change in momentum flow rate due to the effects of mass generation and consumption by the electrochemical reaction.

For fully developed flow with mass transfer, the Nusselt number can be derived from an energy balance in the duct. As mentioned earlier, the mass flow

through the porous wall is much smaller than the main flow, and the total heat flow rate q'_b (per unit length of the duct) can then be calculated by (Figure 2):

$$q'_b = \rho U_{bulk} c_p A \frac{dT}{dx} - \rho c_p V_m a \left(T_{bulk} - T_w\right) \tag{46}$$

This equation can be rearranged for a rectangular duct as:

$$\frac{q'_b}{T_{bulk} - T_w} \frac{D_h}{kP*} = \frac{\rho U_{bulk} c_p A \frac{dT}{dx}}{\left(T_{bulk} - T_w\right)} \frac{D_h}{kP*} - \rho c_p V_m a \frac{D_h}{kP*} \tag{47}$$

The left hand side is the definition for the *Nu* and the first part on the right hand side is the definition of the Nusselt number without mass transfer (Nu_f).

$$Nu = \frac{q'_b D_h}{(T_{bulk} - T_w) kP*} \tag{48}$$

$$Nu_f = \frac{\rho U_{bulk} c_p A \frac{dT}{dx} D_h}{\left(T_{bulk} - T_w\right) kP*} \tag{49}$$

where T_w, the wall temperature, is the same on three walls but varies on the fourth wall for *TBC-I*. T_{bulk} is the bulk flow mean temperature in the cross section, and is calculated as

$$T_{bulk} = \frac{\int T|U|dA}{\int |U| dA} \tag{50}$$

The second part of eqn (47) is the contribution to the Nusselt number by mass transfer. This term is rewritten as

$$Nu_m = -\Pr \mathrm{Re}_m \frac{b}{P*} \tag{51}$$

Eqn (47) is then rewritten as:

$$Nu/Nu_f = 1 + Nu_m/Nu_f \tag{52}$$

The Nusselt number Nu_w can be defined as:

$$Nu_w = \frac{h_w D_h}{k} = \frac{q_w D_h}{k(T_w - T_{bulk})} \tag{53}$$

$$\overline{Nu}_w = \frac{\overline{h}_w D_h}{k} = \frac{q_w D_h}{k(\overline{T}_w - T_{bulk})} \tag{54}$$

where Nu_w and $\overline{Nu}_w$ are spanwise variable and average Nusselt numbers of the heated wall at location x, respectively. q_w is the wall heat flux; T_w and $\overline{T}_w$ are spanwise variable and average temperature of the heated wall, respectively. The dimensionless axial distance x^* in the flow direction for the hydrodynamic entrance region is defined as:

$$x^* = x/(D_h \mathrm{Re}) \tag{55}$$

Mass transfer effects on the friction factor and Nusselt number are shown in Figure 3 for a rectangular duct with TBC-I. For the case of mass injection from the porous wall, additional mass is induced to the duct and thus the axial velocity

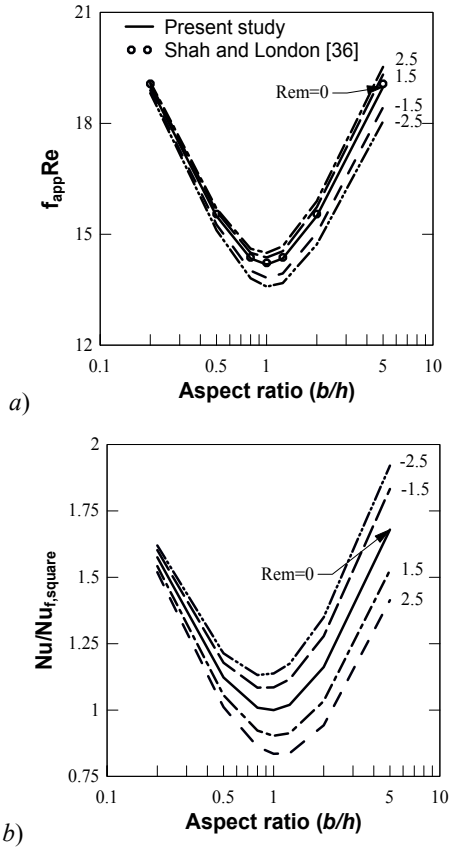

Figure 3: Mass transfer (Re_m) effects on the fully developed convective flow: *a*) the apparent friction factor; and *b*) Nusselt number in a rectangular duct at *TBC-I*, SOFC.

increases. As clarified earlier, the $f_{app}Re$ is related to the pressure gradient as well as changes in the momentum flux in the main flow direction. As can be seen from Figure 3*a*, $f_{app}Re$ always increases for mass injection ($Re_m > 0$), while it decreases for mass suction ($Re_m < 0$). On the other hand for heat transfer, the temperature of the fluid will increase due to the heat induced by mass injection into the fluid, while a decrease appears for the case of mass suction. The Nu/Nu_f is thus reduced by mass injection, which can be seen in Figure 3. A large aspect ratio has a significant effect on both $f_{app}Re$ and Nu/Nu_f, while a small aspect ratio gives less effect. Both $f_{app}Re$ and Nu/Nu_f approach the values for the case without mass transfer ($Re_m = 0$), if the aspect ratio becomes about 0.1. The figures show also that the $f_{app}Re$ and Nu/Nu_f has a minimum when the aspect ratio is unity, i.e., a square duct. More discussion can be found in [35].

Comparisons of $f_{app}Re$ and Nu for a developing flow with and without mass transfer in a rectangular duct are shown in Figure 4 with *TBC-II*. It is clear that the apparent friction factor $f_{app}Re$ is decreased while the Nusselt number Nu is increased. More discussion can be found in [35, 45].

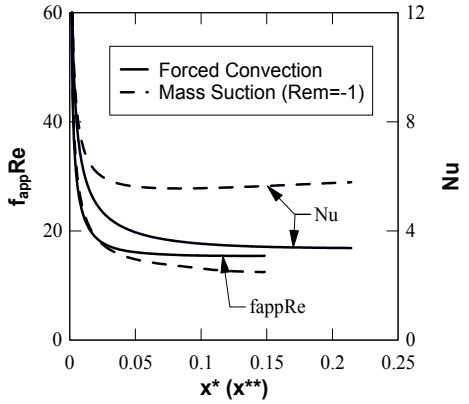

Figure 4: Mass transfer effects on $f_{app}Re$ and Nu for developing flow and heat transfer in a rectangular duct (aspect ratio 2:1) at Re = 250, $Re_m = -1$, *TBC*-II, SOFC.

6.2 Porous layer effects on the transport processes

6.2.1 Transport processes in PEMFCs

In this section, the gas flow and heat transport in a porous layer are included for PEMFCs. The geometry of the duct considered is similar to that in [19, 20], i.e., overall channel dimension is 10 cm × 0.20 cm × 0.16 cm ($x \times y \times z$), gas flow duct is 10 cm × 0.12 cm × 0.08 cm ($x \times y \times z$), while the diffusion layer is 10 cm × 0.04 cm × 0.16 cm (x × y × z). The thickness ratio h_r (thickness of porous layer

Table 1. Parameters implemented as the base case in the PEMFC study.

Cases	Parameter	Value	Reference
Anode inlet	Mole fraction of H_2 / water vapor H_2O / T_{in}, °C	0.53/0.47/ 80	[20]
Cathode inlet	Air with T_{in}, °C	80	[20]
Operating condition	Permeability of diffusion layer β, m^2	2×10^{-10}	[20]
	Porosity ε	0.7	[19]
	Cell voltage V_{cell}, V	0.53	[20]
	Net water transport coefficient α	0.3	[19]
	Current collector thermal conductivity k, W/mK	5.7	[20]

h_{diff} over total height h of the channel) is 20%. The CFD procedure used is modified accordingly and the source term S_m is implemented in the pressure correction equation to adjust the mass balance due to mass transfer. The conditions and parameters considered as the base case are shown in Table 1, along with the references for the various parameters used in the model.

The local current density I of the cell is essential for source term calculations. Because the gas flow and heat transfer in the porous layer and flow ducts are of major interest initially, the approach used in [21] is adopted by prescribing a local current density at the porous layer surface close to the catalyst layer (bottom surface in the study). It should be mentioned that this limitation is abandoned in the following section, where the local current density will be calculated. For a similar geometry, the width-average local current density profiles along the duct length in [19] are adapted to account for various operating conditions (co-/ counter-flow, humid/dry air, membrane thickness and cell voltage). The current density of the base case in this study refers to the case by Yi and Nguyen [19], while the current densities of cases 1, 2 and 3 correspond to cases 1.0, 1.1 and 1.2 from [19], respectively. The current density of the base case is the largest, and case 3 represents the smallest one while the remaining cases have current densities in between the others. A parameter study with various constant current densities has also been performed.

Figure 5*a* presents porous layer thickness effects on the main flow velocity profile (close to the exit) for a fixed value of the permeability ($\beta_i = 2.0 \times 10^{-10}$). The heights of the gas flow duct and solid current collector are kept constant, and the thickness ratio h_r is approached by varying the porous layer thickness and the total height of the duct. It is obvious that the fluid velocity in the porous layer decreases significantly by increasing the thickness of the porous layer. Figure 5*b* corresponds to the case where the thickness of the porous region equals 20 percent of the duct height and the effect of permeability is shown. Clearly, in the porous layer the fluid flow rate is low, and it becomes significantly reduced when the permeability is low (e.g., $\beta_i = 2.0 \times 10^{-11}$). However, the corresponding velocity profiles in the gas flow duct look very similar (see Figure 5*b*).

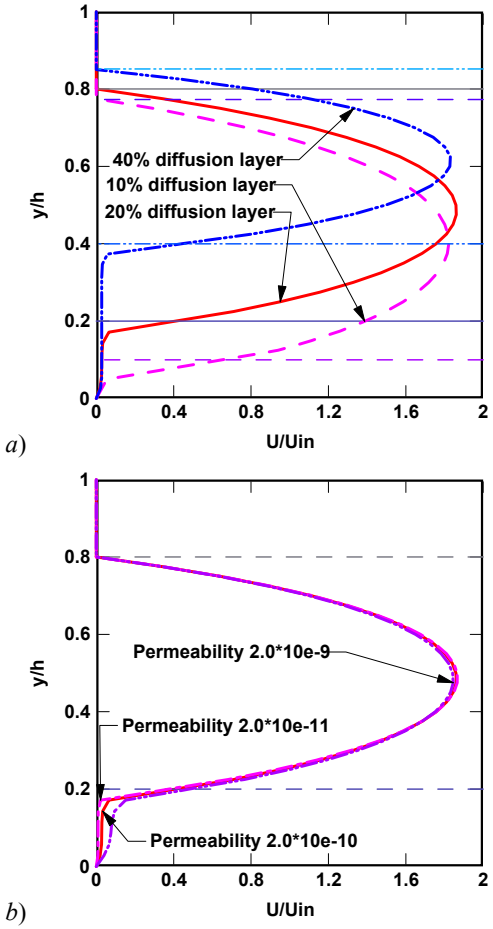

Figure 5: Effects of: *a*) thickness; and *b*) permeability of porous layer on axial velocity profiles in the cathode duct at θ_k (= k_{eff}/k_f) = 1, PEMFC.

In Figure 5*a*, it is noticed that the velocity gradient at the interface region between the porous layer and gas flow duct becomes sharper as the thickness ratio of the diffusion layer increases. As a result, a larger $f_{app}Re$ can be found in Figure 6*a* with a larger thickness ratio of the porous layer (i.e., 40%). Compared to Figure 6*a*, it is found that the permeability at constant thickness ratio has less effect on $f_{app}Re$, which is consistent with the small effect of permeability on the velocity gradient at the interface region, shown in Figure 6*b*.

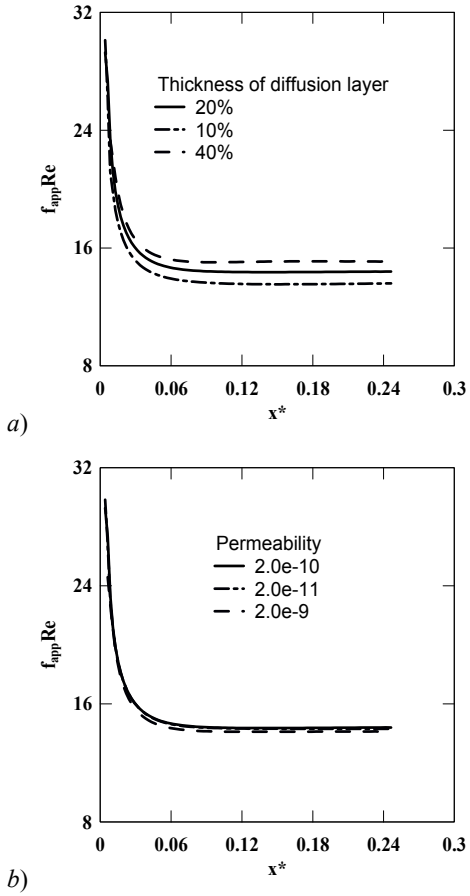

Figure 6: Effects of: a) thickness*;* and b) permeability of the porous layer on $f_{app}Re$ of cathode duct at θ_k =1, PEMFC.

The effects of various current densities on the cross-sectional averaged *Nu* are shown in Figure 7*a*. As seen here, *Nu* of the base case is smaller than those of other cases. A large current density (i.e., base case) can contribute to a large net mass injection to the duct, and to a bigger temperature difference between the heated surface and fluid because more mass and thermal energy are inserted into the duct by the mass injection. A parameter study for various overall current densities with constant values has been performed, and the results are also shown in Figure 7*a*. The conclusion is that a large current density (1.5 A/cm^2 in Figure 7*a*) affects the decrease of Nu_b. Figure 7*b* shows *Nu* with various permeabilities at a fixed current density (base case) and other porous layer parameters for the cathode duct. It is found that by increasing the permeability ($\beta_I = 2.0 \times 10^{-9}$) *Nu* will increase, otherwise *Nu* will decrease [45].

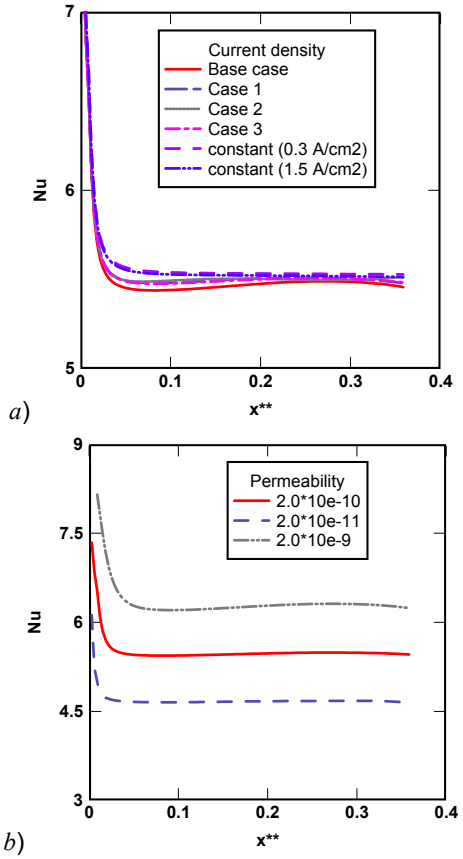

Figure 7: Effects of: a) current density; and b) permeability on *Nu* along the main flow direction of the cathode duct at Re = 300, θ_k = 1.0, h_r = 20%, PEMFC.

As mentioned earlier, there exist some studies in the available literature modifying the Darcy model limitations. For example, the term accounting for friction due to macroscopic shear was included in the model. This model is usually referred to as the Brinkman-extended Darcy (BD) model. It was also suggested that a term representing the inertial energy of the fluid should be included in the Darcy's model and this is often referred to as the Forchheimer term [29, 40]. The inertial coefficient B in eqn (18) depends very much on the microstructure or nanostructure of the porous medium, and theoretical determination of it is not easy. As an example, two models from the literature concerning B are given in Table 2. It is clear that model 2 in the Table needs more detailed information about the porous medium microstructure or nanostruc-

Table 2. The inertial coefficient B in eqn (18).

Model	The inertial coefficient	References
BFD-1	$B = \varepsilon F/(K)^{0.5}$	[29, 40, 41, 42]
BFD-2	$B = 1.75(1-\varepsilon)/(\varepsilon^3 d)$	[43]

ture in a PEMFC, e.g., particle diameter d, which is not available at the present moment. Therefore, only model 1 is used here. Table 3 shows methods how to determine the Forchheimer coefficient F in model 1. Both methods have been adopted in this study, together with a parametric study.

Table 3. The Forchheimer coefficient F in BFD-1 model.

Model	The Forchheimer coefficient	Reference
BFD-1a	$F = 1.8/(180\varepsilon^5)^{0.5}$	[29]
BFD-1b	$F = 0.143\varepsilon^{-1.5}$	[40]

Figures 8*a* and *b* show the variations of the apparent friction factor ratio $f_{app}Re/f_dRe$ (where f_d is the friction factor for fully developed flow) and the Nusselt number Nu along the axial direction with various models. It is clear that both $f_{app}Re/f_dRe$ and Nu rapidly decay due to both the hydrodynamic and thermodynamic boundary layer development. Compared to the BD model, the generalized BFD models predict a larger apparent friction coefficient and a smaller Nu for the PEMFC cathode duct, as seen in Figures 8*a* and *b*. This is because the additional inertial force due to the Forchheimer term (B) retards the side-flow through the porous layer thereby allowing the axial velocity and its gradient to increase. A similar effect occurs due to mass injection into the duct.

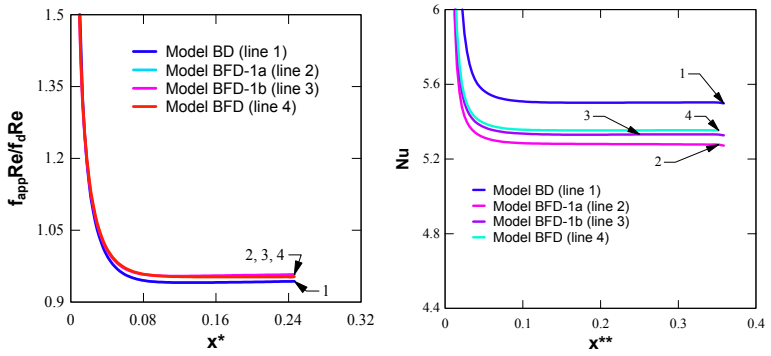

a) *b*)

Figure 8: *a*) $f_{app}Re$; *b*) Nu of a cathode duct by generalized BD and BFD models.

On the other hand, the retarded flow from the porous layer induces more heat into the duct. It is worth noting that the BFD model has significant effects on the decrease of *Nu*, but has small effects on the increase of $f_{app}Re$. It is also clear that both BFD-1*a* and 1*b* models provide similar results for *Nu*, which are close to that at $F = 10^4$ in the figure. From Table 3, it can be verified that the Forchheimer coefficient F from both models is in the order of 10^4 for this specific PEMFC case ($\varepsilon = 0.7$) [46, 47].

Parametric studies of the inertial effects, in terms of the Forchheimer coefficient F, have been conducted for a wide range, covering PEMFC cases. Results are shown in Figures 9*a* and *b*. With reference to $f_{app}Re$ in Figure 9*a*, it is noticed that an increase of F (BFD Models vs BD Model) can increase $f_{app}Re$, but all the cases previde similar $f_{app}Re$, i.e., the Forchheimer coefficient F has a limited effect on $f_{app}Re$. On the other hand for heat transfer, significant changes of *Nu* are expected by increasing the Forchheimer coefficient F, i.e., the inertial force with a larger Forchheimer coefficient forces more gas from the porous layer to the flow duct. Consequently, more heat induced by the retarded flow can be transferred into the duct from the heated wall, and the convective heat transfer coefficient, *Nu*, decreases, see Figure 9*b*.

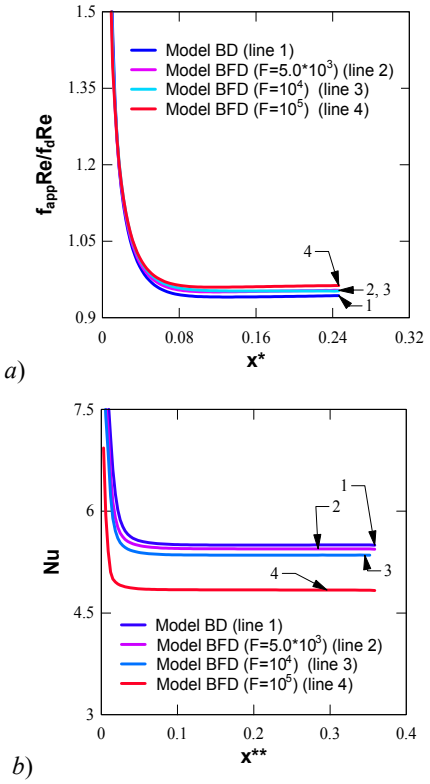

Figure 9: Effects of the inertial energy on: *a*) $f_{app}Re$; and *b*) *Nu* of a cathode duct predicted by the generalized BFD models, PEMFC.

6.2.2 Transport processes in SOFCs

For anode-supported SOFCs, the following duct geometries are employed [9]: length of the duct L = 20 mm; width of the porous layer a = 2 mm, and its thickness h_p = 2 mm; while the width of the flowing duct b = 1 mm, and its height h_d = 1 mm. Fuel gas is 0.80 in mass fraction of H_2, and 0.20 of water vapor with an inlet temperature T_{in} = 750 ^{o}C; thermal conductivity ratio k_r(= k_{eff}/k_f) = 1, effective dynamic viscosity $\mu_{eff} = \mu_f$; porosity $\varepsilon = 0.5$ and permeability $\beta_I = 1.7\times10^{-10}$ m^2; $Re_{in} = 100$, $Re_m = 1.0$, $D_{H2,f} = 3\times10^{-4}$ m^2/s.

Figure 10 shows the permeation Reynolds number Re_p, the friction factor $f_{app}Re$ and the Nusselt number Nu along the main flow direction of an anode-supported SOFC duct. Similar to the wall Reynolds number Re_m (for mass transfer across the bottom wall), the permeation Reynolds number is defined as $Re_p = V_p D_h/\nu$ for gas permeation across the interface. Here, V_p is the velocity caused by the gas permeation across the interface. It is found that Re_p has a large negative value (i.e., permeation into the porous anode layer) at the inlet region, see Figure 10*a*. Due to the decreasing pressure gradient along the duct, permeation into the porous layer becomes smaller. On the other hand, H_2O generation caused by the electrochemical reaction at the bottom wall, together with back permeation described above, contributes to a mass injection into the flow duct. This is confirmed by a small but positive (i.e., back flow into the flow duct) Re_p shortly downstream the inlet in Figure 10*a*.

For a pure flow duct with impermeable walls, $f_{app}Re$ decays rapidly from the inlet, and levels off to a constant value as the convective gas flow becomes fully developed (see Figure 10*b*). For the anode duct with a porous layer, the friction factor, $f_{app}Re$, is small at the inlet region but increases rapidly at the entrance region and also levels off to a near-constant value shortly downstream along the main flow direction. Similar to a suction flow from a duct, there is certainly a decrease in the friction factor from that of the pure forced convection, as mentioned before.

For increasing x^*, the Re_p becomes smaller and its contribution to the decrease of $f_{app}Re$ is less significant. This contribution will be zero when $Re_p = 0$. Along the flow direction beyond this position, the gas flow is possibly affected by the following mechanisms: secondary flow and back permeation to increase $f_{app}Re$, convective flow to decrease $f_{app}Re$. It can be clearly observed that $f_{app}Re$ in Figure 10*b* is nearly constant downstream from the entrance region. Further downstream in the flow duct, the secondary flow and back permeation balance each other and the effects on the main flow disappear. The Nu for the composite duct has a similar behaviour as that of the pure flow duct. However, a slightly bigger Nu can be observed for the composite duct (see Figure 10*b*), due to the mass permeation into the porous layer. From the discussion above, it is clear that mass permeation across the interface has more significant effects on the gas flow than on the heat transfer, both in the entrance region and further downstream.

H_2 and H_2O concentration profiles along the main flow direction are shown in Figures 11*a* and 11*b*, respectively. It is found that the H_2 concentration decreases, while H_2O increases along the main flow in the porous layer and the flow duct. This is due to the consumption of H_2 and generation of H_2O during

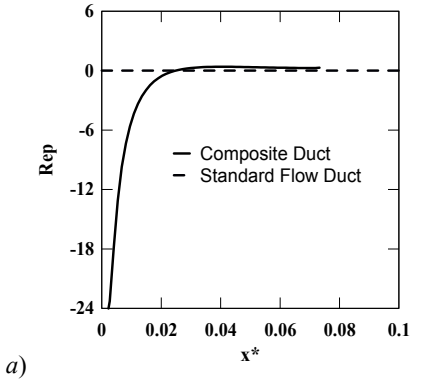

a)

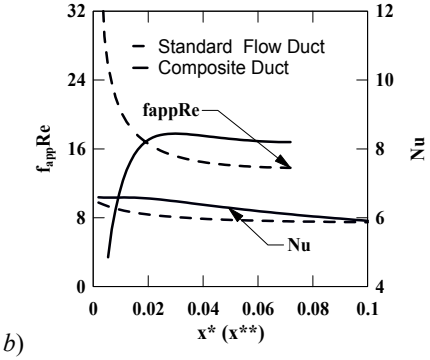

b)

Figure 10: *a*) Permeation Reynolds number Re_p; *b*) $f_{app}Re$ and *Nu* along the main flow direction at the base case condition, SOFC.

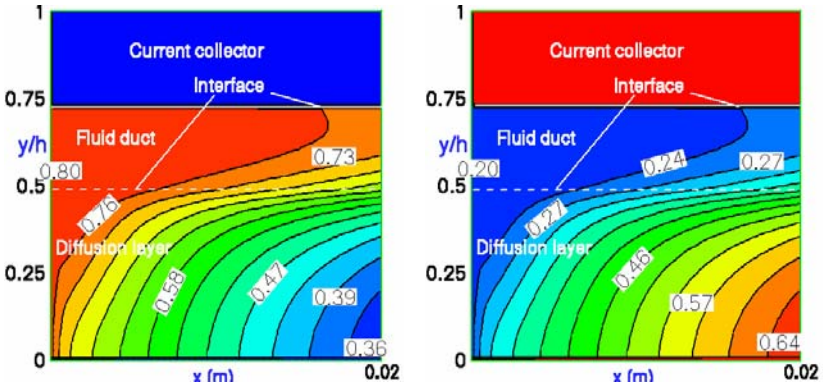

a) *b*)

Figure 11: *a*) H_2; and *b*) H_2O mass concentration distribution along the main flow direction of an SOFC anode duct.

the electrochemical reaction. Moreover, the gradients of the H_2 and H_2O concentrations in the direction normal to the active surface (the bottom surface in Figure 11) are larger close to the reaction sites compared to the interface areas of both porous layer and flow duct [48].

The performance of the anode-supported SOFC duct is also analysed using the vertical component of the total hydrogen mass flux vector at the active site (bottom surface), which can be expressed as:

$$\left(J_{H_2,y}\right)_b = \left(\rho_{eff} m_{H_2} V + \rho_{eff} D_{H_2,eff} \frac{\partial m_{H_2}}{\partial y} \right)_b \tag{56}$$

It should be noted that the first term on the right hand side represents the convection transport, while the second term is the contribution due to the diffusion. Figure 12 shows a comparison of the hydrogen mass fluxes by convection, diffusion and the total value for the base condition. It can be seen that convection mass flux has a large negative value (i.e., fuel species transport is to the reaction sites) at the inlet region. Due to the decreasing pressure difference along the duct, convection becomes weaker downstream. On the other hand, water generation caused by the reaction at the active sites, together with the back permeation mentioned above, contributes to species flowing back to the flow duct. This is confirmed by a small positive value of the convection flux. It is also clear that the hydrogen diffusion flux is small in the entrance region due to a small hydrogen concentration gradient as discussed above, but it increases and reaches a peak value at a certain position of the duct. This is caused by the reaction. The diffusion flux maintains almost a constant value further downstream.

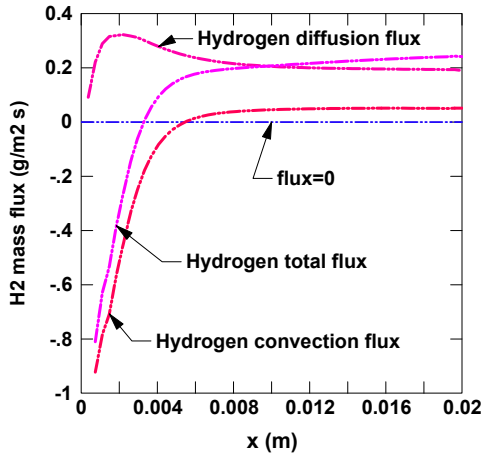

Figure 12: Various modes of hydrogen flux at the active surface for the base case condition, SOFC.

By comparing the absolute values of convection and diffusion fluxes, it is

found that the convection is stronger in the entrance region; however, the diffusion dominates the species transport downstream. The position for this occurrence is about 1/6 length from the inlet for this specific case. Consequently the total flux from eqn (56) is controlled by convection in the entrance region, and by diffusion for the rest of the duct, as seen in Figure 12.

6.3 Two-phase flow and its effects on the cell performance

As mentioned earlier, the important feature of the two-phase flow model implemented in the work described in this chapter is based on the two-phase mixture approach to account for the phase change and its effects on the gas flow and heat transfer. The approach is to model the liquid water transported by the multi-component gas mixture in terms of the convection and the diffusion. The amount of water undergoing phase-change is calculated based on the partial pressure of water vapor and the saturation pressure. It is worthwhile to note that two-phase flow and heat transfer are concerned to get local pressure, temperature and species component composition. The model is therefore considered as a non-isothermal and -isobaric model. As mentioned above, the source term in eqn (21) is for the water phase change. When the partial pressure of water vapor is greater than the saturation pressure, water vapor will condense to liquid water. Consequently, the mass fraction will be reduced in the main gas flow, together with a release of water latent heat, which continues to occur until the partial pressure equals the local saturation pressure. On the other hand, if the partial pressure is lower than the saturation pressure, the saturated water, if any, will evaporate. It should be mentioned that the source term in eqn (22) concerning the water phase-change and the associated heat source term in eqn (20) correspond to the control volumes where two-phase water appears, and these are not treated as the boundary conditions.

In this section, the main results of numerical simulations are reported and discussed for a cathode duct of PEMFCs. Figure 13*a* shows the velocity profile along the main flow direction, in which the scale of the vector plots (i.e., 2 m/s) is a reference value of the maximum velocity. As shown in the figure, a parabolic profile is clearly observed in the flow duct. On the other hand, because the species have difficulties penetrating into the porous layer, the velocity in the porous layer is very small except in the region close to the flow duct.

Figure 13*b* shows that the temperature increases along the main flow direction. The variation in temperature distribution can also be observed in the vertical direction with a slightly larger value close to the bottom surface. These effects are created by the heat generation due to both the reaction close to the active surface, and the latent heat release by water condensation in the two-phase region, caused by the increase in the water vapor concentration in this area. It is worthwhile to note that the temperature is non-uniformly distributed. By considering the local temperature distribution, the effects on the saturation pressure can be found, which is not the case for the isothermal assumption employed by different authors in literature [49].

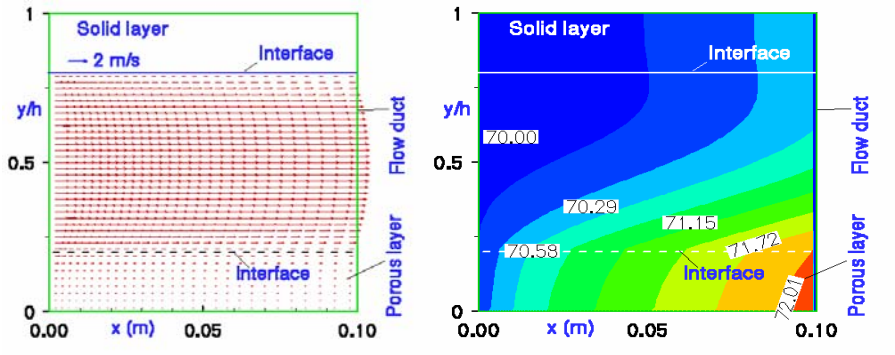

a) *b*)

Figure 13: *a*) Velocity vectors; and *b*) contours of temperature T along the main flow direction of a composite duct, PEMFC.

Water activities in the duct are shown in Figure 14. The mass concentration of the water vapor at the entrance is 23%, which corresponds to the saturated case at the base condition (T_{in} = 70 °C). It can be observed that water vapor is generated at the bottom surface, and is transported back to the flow duct through the porous layer. For this reason, larger mass fractions of water vapor can be found in the porous layer close to the bottom surface. Therefore, the partial pressure of water vapor is greater in the regions mentioned above, and smaller at the interfacial region and the flow duct. Based on the calculated partial pressure and the saturation condition, the liquid water content was predicted and shown in Figure 14*b*. It is found that the liquid water appears in both the flow duct and the porous layer, with the largest mass fraction (around 10%) in the porous layer close to the exit. Because the saturation pressure is proportional to the local temperature, smaller saturated pressures can be expected for the flow duct compared to the porous layer. This is the reason why the liquid water can appear in the flow duct as well, but with smaller mass fractions (less than 5%). A proper gradient of the liquid water concentration should be kept for the liquid water to be driven out of the porous layer.

Figure 15 shows the corresponding liquid water saturation level along the main flow direction of the composite duct. As shown in eqn (36), liquid saturation is represented by the volume occupied by the liquid phase divided by the total flow volume of the duct. It is clear that the liquid saturation s is zero in the single-phase gas flow region. It is so because the species density reduces to the gas phase density, and the water mass fraction equals the mass fraction of the water vapor as well. The liquid saturation s is 1.0 for the case of the single-phase liquid flow. As shown in Figure 15, the liquid saturation s is zero in the inlet region and increases along the flow direction. It is also true that the liquid saturation s decreases from the active site to the flow duct at the same x due to the liquid water transport, as discussed later in this paper. The liquid water occupies more volume in the porous layer with the largest value of s appearing

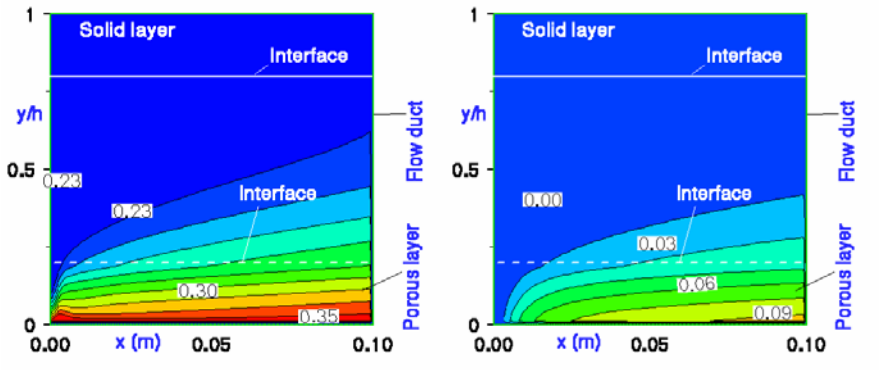

a) *b*)

Figure 14: Mass concentration profiles for: *a*) water vapor; and *b*) liquid water along main flow direction of PEMFC cathode duct at the base case.

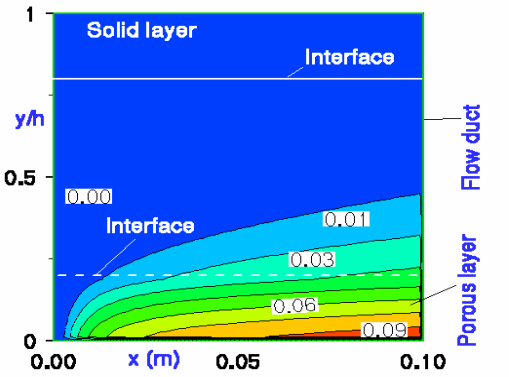

Figure 15: Liquid saturation profile along the main flow direction in a composite duct at the base case, PEMFC.

in the corner close to the active surface at the exit of the duct, while the single-phase gas species occupy most of the flow duct except that small values of s can be observed at the interface region after a certain distance downstream the inlet.

As discussed above, the liquid water mass composition and saturation level have highest values at the active surface, consequently larger contribution to the species flow and heat transfer can be expected. In this section, the liquid water flow in the porous layer is evaluated by the liquid water mass flux at the active site, as shown in eqn (56). It should be noted that a positive value represents liquid water flowing from the active site to the porous layer and then the flow duct.

Figure 16*a* shows the comparison of the liquid water mass fluxes by convection, diffusion and the total value for the base case. It is found that both convection and diffusion mass fluxes have very small values at the inlet region.

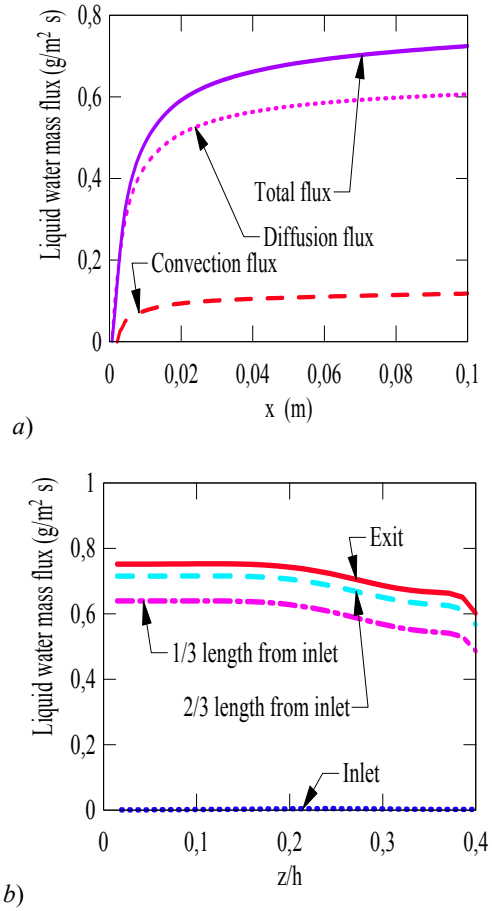

Figure 16: Liquid water flux at the active surface for: *a*) the main flow direction; and *b*) the cross-sections in a composite duct for the base case, PEMFC.

Due to the phase change, when the water vapor is generated and the saturation condition is reached, the liquid water can be accumulated in this region. Its mass concentration and gradient along the duct become larger. Bigger values can therefore be observed for both the convection and diffusion downstream a certain distance from the inlet. As shown in Figure 16*a*, the saturated water transport is dominated by diffusion which takes place mainly in the porous layer. In fact, the convective contribution to the total water flux is estimated to be about 15% or less. Consequently the total flux from eqn (56) can be said to be controlled by the diffusion for this specific case.

Figure 16*b* shows the predicted total values of the cross-sectional liquid water mass flux at various locations. As shown, the mass flux is zero at the inlet region. It is found that the total mass flux has almost uniform values in the cross sections, except a weak liquid water flow for the site below the solid layer (z/h = 0.2~0.4), which has a long transport distance from/to the flow duct [50].

As mentioned previously, the local current density (I) is an important parameter of the cell, and essential for the source term calculations related to mass injection/suction and heat generation by the electrochemical reaction. In this section, the local current density is calculated considering the effects of the liquid water saturation, and can be expressed as follows,

$$I = I_o \left[\frac{(1-s)\phi_{O_2}}{\phi_{O_2,ref}} \right]_b \exp\left(-\frac{O_{2,trans} F}{RT} V_{over} \right) \tag{57}$$

where I is the local current density based on the Tafel equation along the active surface, I_o the exchange current density per real catalyst area, ϕ_{O_2} the oxygen species mass concentration, $O_{2,trans}$ the transfer coefficient for the oxygen reaction, V_{over} the cathode over-potential, $\phi_{O_2,ref}$ the oxygen reference concentration (e.g., P = 1 atm) for the oxygen reaction. Other symbols are given in the nomenclature. The $(1 - s)$ factor in eqn. (57) accounts for the effect of liquid water saturation on the surface availability of the reaction site.

Figure 17*a* shows a local current density distribution on the active surface (in the x–z plane). It can be seen that the current density is high near the entrance, and then decreases along the main flow direction. This is because the oxygen transfer to the reaction site is larger near the entrance region, which is dominated by the oxygen convection. The reduced current density downstream is due to the small oxygen transport rate controlled by the diffusion. It is also true that the current density is non-uniformly distributed in the cross-section with a smaller value in the corner region beneath the solid current collector. This is due to a longer transport distance from the flow duct to the active site. With reference to Figure 17*b*, a similar conclusion can be drawn, i.e., the current density is non-uniform along the main flow direction and in the cross-section as well. It should be noted that the liquid water saturation affects this non-uniform distribution as indicated by eqn (57).

The simulation results from a 3-D PEMFC model developed in [52] are compared with experimental data available for various parameters. Figure 18 shows a typical V-I polarization curve at operating and humidification temperatures of 70 ^{o}C on both the anode and cathode sides. From the figure it is found that the comparison is favorable at low and medium current densities, but this is not true for the case for the high current densities. It is obvious that the simulation produces a higher current density. As claimed in [52], the low current density of the experimental results may be caused by the presence of liquid water

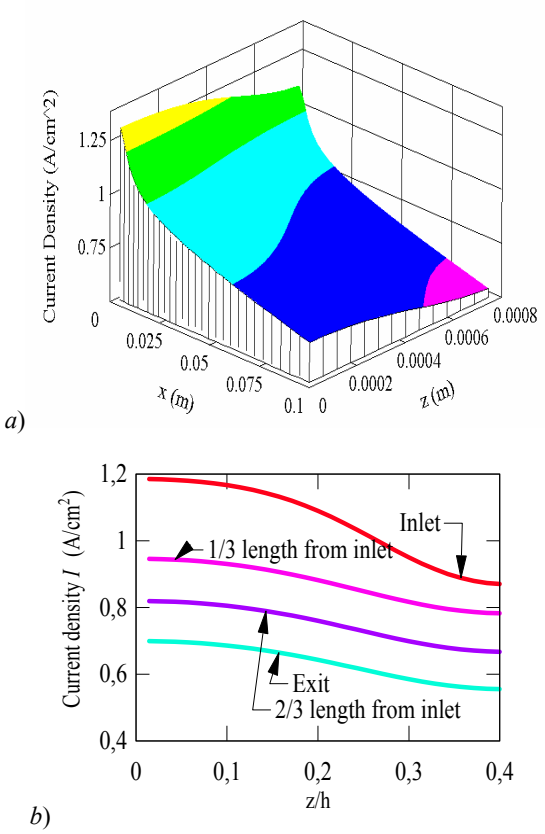

Figure 17: Local current density distribution for: *a*) the active surface; and *b*) the cross-sections in a cathode duct of a PEMFC at the base case.

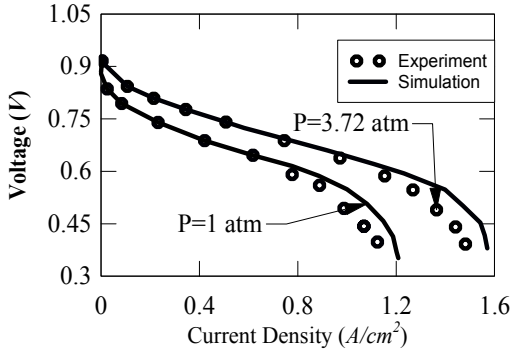

Figure 18: Comparison of the calculated results with the experimental data for polarization curves (*V-I* curve) of PEMFC, from [52].

content in the catalyst layers and the gas diffusion layers, which the model employed in [52] neglected.

7. Conclusions

Based on the similarities of major transport processes in SOFCs and PEMFCs, a unified framework of computational fluid dynamics (CFD) methodology has been developed by implementing specific source terms to account for transport processes and boundary conditions. Numerical investigations and analyses for species flow and heat transfer have been presented for ducts of the type appearing in fuel cells. Models were developed for ducts with the thermal boundary conditions appearing in SOFCs and PEMFCs. Also, different duct configurations were considered, such as rectangular and trapezoidal cross sections, and composite geometries including porous layer, flow duct and solid current inter-collector. It was found that the electrochemical reaction related mass consumption/generation in the electrodes, duct configuration (such as the characteristics of the porous layer) have major effects on the gas flow and heat transfer. Furthermore, water management involving two-phase flow in PEMFCs has been studied, and its importance for the cell performance has been characterized.

Acknowledgement

Financial support was provided by the Swedish National Programme for Stationary Fuel Cells. The Swedish Energy Agency (STEM) is the financial supporter and Elforsk is handling the programme. The Wenner-Gren Foundation supported the collaboration between Professors Faghri and Sundén.

Nomenclature

A	area, m^2
a	width of porous layer, m
b	width of flow duct, m
B	microscopic inertial coefficient, 1/m
BD	Brinkman-extended Darcy model
BFD	Brinkman-Forchheimer-Darcy model
d	sphere diameter of porous layer, m
c_p	specific heat, J/(kg K)
D	diffusion coefficient, m^2/s
D_h	hydraulic diameter, m
D_{hr}	diameter ratio
f_{app}	apparent friction factor
F	Faraday constant (96487 C/mol) or the Forchheimer coefficient
H	enthalpy, J/kg
h_b	heat transfer coefficient, $W/(m^2 K)$
h_d	height of the duct, m

h_p	thickness of porous layer, m
h_r	thickness ratio (h_p/h_d)
h_{wl}	water latent heat, J/kg
I	current density, A/m^2
J	mass flux of species, kg/(m^2 s) or kg/(m^3 s)
k	thermal conductivity, W/(m K)
k_r	thermal conductivity ratio (k_{eff}/k_f)
M	molecular weight, kg/kmol
MEA	membrane electrolyte assembly
$\overline{Nu}_b$	spanwise average Nusselt number
$O_{2,trans}$	transfer coefficient for the oxygen reaction
P	pressure, Pa
P^*	wetted perimeter, m
q	heat flux, W/(m^2)
q'	heat flow rate per unit length of duct, (W/m)
Re	Reynolds number (UD_h/ν)
Re_m	wall Reynolds number ($V_m D_h/\nu$)
Re_p	permeation Reynolds number ($V_p D_h/\nu$)
S	source term
s	liquid water saturation
S_{di}	source term in momentum equations
T	temperature, ^{o}C
$TBC\text{-}I$	thermal boundary condition I
$TBC\text{-}II$	thermal boundary condition II
U_i	velocity components in x, y and z directions, respectively, m/s
V	volume of control volume at active site, m^3
$\mathbf{v}$	velocity vector, m/s
V_{cell}	cell voltage, V
V_m	mass transfer velocity at bottom wall, m/s
V_p	permeation velocity across interface, m/s
x,y,z	Cartesian coordinates
x^*	hydrodynamic dimensionless axial distance ($x/(D_h Re)$)
x^{**}	thermal dimensionless axial distance (x^*/Pr)

Greek symbols

α	net water transport coefficient
β_i	permeability of diffusion layer, m^2
ε	porosity
ϕ	mass fraction
Φ	arbitrary variable
η	relative humidity, %
μ	dynamic viscosity, kg/(m s)
ν	kinematic viscosity, m^2/s
ρ	density, kg/m^3

Subscripts

a	anode or air
active	at active site
av	average
b	bottom wall
bulk	bulk fluid condition
c	cathode
e	electrolyte
eff	effective parameter
f	fluid or fuel
H_2	hydrogen
H_2O	water vapor
in	inlet
m	mass transfer
O_2	oxygen
out	outlet
p	porous layer or permeation
s	solid layer
w	wall
sat	saturation
wl	water liquid
wp	water phase change
wv	water vapor

References

[1] Haraldsson, K. & Vipke, K., Evaluating PEM fuel cell system models, *J. Power Sources*, 126, pp. 88–97, 2004.

[2] FEMLAB Chemical Engineering, COMSOL documentation, 2002.

[3] Vayenas, C.G., Debenedettl, P.G., Yentekakls, I. & Hegedus, L.L., Cross-flow, Solid-state Electrochemical Reactors: A Steady-State Analysis, *Ind. Eng. Chem. Fundam*., 24, pp. 316–324, 1985.

[4] Ahmed, S., McPheeters, C. & Kumar, R., Thermal-Hydraulic Model of a Monolithic Solid Oxide Fuel Cell, *J. Electrochemical Society*, 138, pp. 2712–2718, 1991.

[5] Bernier, M., Ferguson, J. & Herbin, R., A 3-dimensional Planar SOFC Stack Model, *Proceedings of Third European Solid Oxide Fuel Cell Forum*, Nantes, France, pp. 471–480, 1998.

[6] Melhus, O. & Ratkje, S.K., A Simultaneous Solution of All Transport Processes in a Solid Oxide Fuel Cell, *Denki Kagaku*, 64, pp. 662–673, 1996.

[7] Boersma, R.J. & Sammes, N.M., Distribution of Gas Flow in Internally Manifolded Solid Oxide Fuel-cell Stacks, *J. Power Sources*, 66, pp. 41–45, 1997.

[8] Virkar, A.V., Chen, J., Tanner, C.W. & Kim, J.W., The Role of Electrode

Microstructure on Activation and Concentration Polarizations in Solid Oxide Fuel Cells, *Solid State Ionics*, 131, pp. 189–198, 2000.

[9] Yakabe, H., Hishinuma, M., Uratani, M., Matsuzaki, Y. & Yasuda, I., Evaluation and Modeling of Performance of Anode-supported Solid Oxide Fuel Cell, *J. Power Sources*, 86, pp. 423–431, 2001.

[10] Lehnert, W., Meusinger, J. & Thom, F., Modelling of Gas Transport Phenomena in SOFC Anodes, *J. Power Sources*, 87, pp. 57–63, 2000.

[11] Ackmann, T., Haart, L.G.J., Lehnert, W. & Thom, F., Modelling of Mass and Heat Transport in Thick-Substrate Thin-Electrolyte Layer SOFCs, *Proceedings of the 4th European Solid Oxide Fuel Cell Forum*, Lucerne/Switzerland, pp. 431–438, July 2000.

[12] Yi, J.S. & Nguyen T.V., An Along-the-Channel Model for Proton Exchange Membrane Fuel Cells, *J. Electrochem. Soc*., 145, pp. 1149-1159, 1998.

[13] Nguyen, T.V. & White, R.E., A Water and Heat Management Model for Proton Exchange Membrane Fuel Cells, *J. Electrochem. Soc.*, 140, pp. 2178–2186, 1993.

[14] Singh, D., Lu, D.M. & Djilali, N., A Two-Dimensional Analysis of Mass Transport in Proton Exchange Membrane Fuel Cells, *Int. J. of Eng. Sci*., 37, pp. 431–42, 1999.

[15] Okada, T., Xie, G. & Meeg, M., Simulation for Water Management in Membranes for Polymer Electrolyte Fuel Cells, *Electrochem. Acta*, 43, pp. pp. 2141–2155, 1998.

[16] Kazim, A., Liu, H.T. & Forges, P., Modelling of Performance of PEM Fuel Cells with Conventional and Interdigitated Flow Fields, *J. Applied Electrochem*., 29, pp. 1409–1416, 1999.

[17] Um, S., Wang, C.Y. & Chen, K.S., Computational Fluid Dynamics Modeling of Proton Exchange Membrane Fuel Cells, *J. Electrochem. Soc.*, 147, pp. 4485–4493, 2000.

[18] Voss, H.H., Wilkinson, D.P., Pickup, P.G., Johnson, M.C. & Basura, V., Anode Water Removal: a Water Management and Diagnostic Technique for Solid Polymer Fuel Cells, *Electrochimica Acta*, 40, pp. 321–328, 1995.

[19] Dutta, S., Shimpalee, S. & Zee, J.W.V., Three-Dimensional Numerical Simulation of Straight Channel PEM Fuel Cells, *J. Appl. Electrochemistry*, 30, pp. 135-146, 2000.

[20] Shimpalee, S. & Dutta, S., Numerical Prediction of Temperature Distribution in PEM Fuel Cells, *Num. Heat Transfer (Part A)*, 38, pp. 111–128, 2000.

[21] You, L. & Liu, H. A Two-phase and Multi-Component Model for the Cathode of PEM Fuel Cells, *ASME* IMECE2001/HTD-24273, pp. 1–10, 2001.

[22] He, W., Yi, J.S. & Nguyen, T.V., Two-phase Flow Model of the Cathode of PEM Fuel Cells Using Interdigitated Flow Fields, *AIChE Journal*, 46,

pp. 2053–2064, 2000.

[23] Nguyen, T.V., Modeling Two-Phase Flow in the Porous Electrodes of Proton Exchange Membrane Fuel Cells Using the Interdigitated Flow Fields, *Electrochem. Soc. Proc.*, 99-14, pp. 222–241, 2000.

[24] Wang, Z.H., Wang, C.Y. & Chen, K.S., Two-Phase Flow and Transport in the Air Cathode of Proton Exchange Membrane Fuel Cells, *J. Power Sources*, 94, pp. 40–50, 2001.

[25] Djilali, N. & Lu, D., Influence of Heat Transfer on Gas and Water Transport in Fuel Cells, *Int. J. Therm. Sci*., 41, pp. 29–40, 2002.

[26] Hwang, G.J., Cheng, Y.C. & Ng, M.L., Developing Laminar Flow and Heat Transfer in a Square Duct with One-Walled Injection and Suction, *Int. J. Heat Mass Transfer*, 36, pp. 2429–2440, 1993.

[27] Kinney, R.B., Fully Developed Frictional and Heat-Transfer Characteristics of Laminar Flow in Porous Tubes, *Int. J. Heat Mass Transfer,* 11, pp. 1393–1401, 1968.

[28] Quaile, J.P. & Levy, E.K., Laminar Fow in a Porous Tube with Suction, *ASME J. Heat Transfer,* 97, pp. 66–71, 1975.

[29] Teng, H. & Zhao, T.S., An Extension of Darcy's Law to Non-Stokes Flow in Porous Media, *Chem. Eng. Sci.*, 55, pp. 2727–2735, 2000.

[30] Alkam, M.K., Al-Nimr, M.A. & Hamdan, M.O., Enhancing Heat Transfer in Parallel-Plate Channels by Using Porous Inserts, *Int. J. Heat Mass Transfer,* 44, pp. 931–938, 2001.

[31] Alazmi, B. & Vafai, K., Analysis of Fluid Flow and Heat Transfer Interfacial Conditions between a Porous Medium and a Fluid Layer, *Int. J. Heat Mass Transfer*, 44, pp. 1735–1749, 2001.

[32] Wang, J., Gao, Z., Gan, G. & Wu, D., Analytical Solution of Flow Coefficients for a Uniformly Distributed Porous Channel, *Chem. Eng. Journal*, 84, pp. 1–6, 2001.

[33] Kee, R.J., Korada, P., Walters, K. & Pavol, M., A Generalized Model of the Flow Distribution in Channel Networks of Planar Fuel Cells, *J. Power Sources*, 109, pp. 148-159, 2002.

[34] Versteeg, H.K. & Malalasekera, W., *An Introduction to Computational Fluid Dynamics, the Finite Volume Method*, Longman Scientific & Technical, England, 1995.

[35] Yuan, J., *Computational Analysis of Gas Flow and Heat Transport Phenomena in Ducts Relevant for Fuel Cells*, Ph.D. Thesis, ISBN 91-628-5540-9/ISSN 0282-1990, Lund Institute of Technology, Sweden, 2003.

[36] R.K. Shah, A.L. London, Laminar Flow Forced Convection in Ducts (Chapters VII and X), in: *Advances in Heat Transfer*, eds. T.F. Irvine and J.P. Hartnett, Academic Press: New York, 1978.

[37] Comiti, J., Sabiri, N.E. & Montillet, A., Experimental Characterization of Flow Regimes in Various Porous Media-III: Limit of Darcy's or Creeping

Flow Regime for Newtonian and Purely Viscos Non-Newtonian Fluids, *Chem. Eng. Sci*., 55 pp. 3057–3061, 2000.

[38] Natarajan, D. & Nguyen, T.V., A Two-Dimensional, Two-Phase, Multicomponent, Transient Model for the Cathode of a Proton Exchange Membrane Fuel Cell Using Conventional Gas Distributors, *J. Electrochem. Soc*, 148, pp. A1324–1335, 2001.

[39] Warnatz, J., Maas, U. & Dibble, R.W., *Combustion-Physical and Chemical Fundamentals, Modeling and Simulation, Experiments, Pollutant Formation*: Springer, Berlin, Germany, 1996.

[40] Chikh, S., Bounedien, A. & K. Bouhadef, Non-Darcian Forced Convection Analysis in an Annulus Partially Filled with a Porous Material, *Num. Heat Transfer*, 28, pp. 707–722, 1995.

[41] Marafie, A., & K. Vafai, Analysis of Non-Darcian Effects on Temperature Differentials in Porous Media, *Int. J. Heat Mass Transfer*, 44, pp. 4401–4411, 2001.

[42] Vafai, K. & Kim, S.J., Fluid Mechanics of the Interface Region Between a Porous Medium and a Fluid Layer – An Exact Solution, *Int. J. Heat Fluid Flow,* 11, pp. 254–256, 1990.

[43] Poulikakos, D. & Renken, K., Forced Convection in a Channel Filled With Porous Medium, Including the Effects of Flow Inertial, Variable Porosity, and Brinkman Friction, *ASME J. Heat Transfer*, 109, pp. 880–888, 1987.

[44] Yuan, J., Rokni, M. & Sundén, B., Simulation of Fully Developed Laminar Heat and Mass Transfer in Fuel Cell Ducts with Different Cross Sections, *Int. J. Heat Mass Transfer*, 44, pp. 4047–4058, 2001.

[45] Yuan, J., Rokni, M. & Sundén, B., A Numerical Investigation of Gas Flow and Heat Transfer in Proton Exchange Membrane Fuel Cells, *Num. Heat Transfer*, 44, pp. 255–280, 2003.

[46] Yuan, J., Rokni, M. & Sundén, B., Three-Dimensional Computational Analysis of Gas and Heat Transport Phenomena in Ducts Relevant for Anode-Supported Solid Oxide Fuel Cells, *Int. J. Heat Mass Transfer*, 46, pp. 809–821, 2003.

[47] Yuan, J. & Sundén, B., A Numerical Investigation of Heat Transfer and Gas Flow in Proton Exchange Membrane Fuel Cell Ducts by a Generalized Extended Darcy Model, *Int. J. Green Energy*, 1, pp. 47–63, 2004.

[48] Yuan, J., Rokni, M. & Sundén, B., Gas Flow and Heat Transfer Analysis for an Anode Duct in Reduced Temperature SOFCs. in: *Fuel Cell Science, Engineering and Technology*, eds. R.K. Shah and S.G. Kandlikar, pp. 209–216, FUELCELL2003-1721, ASME, 2003.

[49] Yuan, J. & Sundén, B., Two-Phase Flow Analysis in a Cathode Duct of PEFCs, *Electrochemica Acta*, 50, pp. 677–683, 2004.

[50] Yuan, J. & Sundén, B., Numerical Simulation of Two-Phase Flow and Heat Transfer in a Composite Duct, IMECE 2003–42228, Proc. of ASME

International Mech. Eng. Cong. and R&D Expo, Washington, DC, CD-ROM, 2003.

[51] Beale, S.B., Some Aspects of Mass Transfer within the Passages of Fuel Cells. in: *Fuel Cell Science, Engineering and Technology*, eds. R.K. Shah and S.G. Kandlikar, pp. 293–300, FUELCELL2003-1721, ASME, 2003.

[52] Wang L., Husar, A., Zhou, T. & Liu, H., A Parametric Study of PEM Fuel Cell Performance, *Int. J. Hydrogen Energy*, 28, pp. 1263–1272, 2003.